GEORGIA DOT RESEARCH PROJECT 23-21

Final Report

MEASUREMENT OF CEMENT CONTENT AND LAYER THICKNESS VARIATION OF CEMENT-STABILIZED BASE AND SUBGRADE USING GROUND PENETRATING RADAR

Office of Performance-based Management and Research
600 West Peachtree Street NW | Atlanta, GA 30308

February 2026

TECHNICAL REPORT DOCUMENTATION PAGE

1. Report No.: FHWA-GA-26-2321	2. Government Accession No.: N/A	3. Recipient's Catalog No.: N/A
4. Title and Subtitle: Measurement of Cement Content and Layer Thickness Variation of Cement-Stabilized Base and Subgrade Using Ground Penetrating Radar		5. Report Date: February 2026
		6. Performing Organization Code: N/A
7. Author(s): S. Sonny Kim (PI), Ph.D., P.E.; Bjorn Birgisson, Ph.D., P.E.; Damilola Arinola; and Zack Hall		8. Performing Organization Report No.: 23-21
9. Performing Organization Name and Address: University of Georgia, College of Engineering Driftmier Engineering Center, Athens, GA 30602 Email: kims@uga.edu		10. Work Unit No.: N/A
		11. Contract or Grant No.: PI#0015304
12. Sponsoring Agency Name and Address: Georgia Department of Transportation Office of Performance-based Management and Research 600 West Peachtree St. NW Atlanta, GA 30308		13. Type of Report and Period Covered: Final Report (October 2023–February 2026)
		14. Sponsoring Agency Code: N/A
15. Supplementary Notes: Prepared in cooperation with the U.S. Department of Transportation, Federal Highway Administration.		

16. Abstract:

This report presents a comprehensive methodology for evaluating cement content and layer thickness variability in cement-stabilized pavement layers using a nondestructive ground penetrating radar (GPR) technique. The research integrates laboratory calibration and field validation for two widely used stabilization practices: conventional soil-cement stabilization and full-depth reclamation (FDR).

Laboratory work involved preparing soil-cement/FDR specimens with varying cement and moisture contents, compacted to field-representative densities. The specimens were tested daily for over an 8-day curing period using dielectric constant and electrical conductivity measurements to track the hydration process. A field GPR survey was conducted at several GDOT project sites in Albany, Conyers, and Peachtree City, as well as Henry County, using a 2-GHz air-coupled antenna. Dielectric constants were obtained from GPR scans, and electrical conductivity was derived through the Crockford et al. (2021) model. Cement content estimation was performed by matching the field electrical conductivity values to the corresponding laboratory-derived surfaces.

The estimated cement content at the soil-cement and FDR sites ranged between 4 and 7 percent. Although some sites showed results consistent with the running average, others exhibited estimated cement contents exceeding or falling below the design mix, indicating non-uniform cement application across the sites. These findings highlight the importance of developing a reliable quality control and quality assurance framework to ensure consistent and verifiable material performance in the field.

17. Keywords: Soil-cement, Full-depth Reclamation, Ground Penetrating Radar, Dielectric Constant, Electrical Conductivity	18. Distribution Statement: No Restriction		
19. Security Classification (of this report): Unclassified	20. Security Classification (of this page): Unclassified	21. No. of Pages: 96	22. Price: Free

Form DOT 1700.7 (8-72) Reproduction of completed page authorized

GDOT Research Project 23-21

Final Report

MEASUREMENT OF CEMENT CONTENT AND LAYER THICKNESS VARIATION OF CEMENT-STABILIZED BASE AND SUBGRADE USING GROUND PENETRATING RADAR

By

S. Sonny Kim, Ph.D., P.E., F. ASCE
Professor[1]

Bjorn Birgisson, Ph.D., P.E., F. ASCE
Professor[1]

Damilola Arinola
Graduate Research Assistant[1]

Zack Hall
Civil Engineer II[2]

[1]Civil and Environmental Engineering, College of Engineering, University of Georgia
[2]Office of Materials and Testing, Georgia Department of Transportation

Contract with
Georgia Department of Transportation

In cooperation with
U.S. Department of Transportation, Federal Highway Administration

February 2026

SI* (MODERN METRIC) CONVERSION FACTORS

APPROXIMATE CONVERSIONS TO SI UNITS

Symbol	When You Know	Multiply By	To Find	Symbol
		LENGTH		
in	inches	25.4	millimeters	mm
ft	feet	0.305	meters	m
yd	yards	0.914	meters	m
mi	miles	1.61	kilometers	km
		AREA		
in^2	square inches	645.2	square millimeters	mm^2
ft^2	square feet	0.093	square meters	m^2
yd^2	square yard	0.836	square meters	m^2
ac	acres	0.405	hectares	ha
mi^2	square miles	2.59	square kilometers	km^2
		VOLUME		
fl oz	fluid ounces	29.57	milliliters	mL
gal	gallons	3.785	liters	L
ft^3	cubic feet	0.028	cubic meters	m^3
yd^3	cubic yards	0.765	cubic meters	m^3
	NOTE: volumes greater than 1000 L shall be shown in m^3			
		MASS		
oz	ounces	28.35	grams	g
lb	pounds	0.454	kilograms	kg
T	short tons (2000 lb)	0.907	megagrams (or "metric ton")	Mg (or "t")
		TEMPERATURE (exact degrees)		
^oF	Fahrenheit	5 (F-32)/9 or (F-32)/1.8	Celsius	^oC
		ILLUMINATION		
fc	foot-candles	10.76	lux	lx
fl	foot-Lamberts	3.426	$candela/m^2$	cd/m^2
		FORCE and PRESSURE or STRESS		
lbf	poundforce	4.45	newtons	N
lbf/in^2	poundforce per square inch	6.89	kilopascals	kPa

APPROXIMATE CONVERSIONS FROM SI UNITS

Symbol	When You Know	Multiply By	To Find	Symbol
		LENGTH		
mm	millimeters	0.039	inches	in
m	meters	3.28	feet	ft
m	meters	1.09	yards	yd
km	kilometers	0.621	miles	mi
		AREA		
mm^2	square millimeters	0.0016	square inches	in^2
m^2	square meters	10.764	square feet	ft^2
m^2	square meters	1.195	square yards	yd^2
ha	hectares	2.47	acres	ac
km^2	square kilometers	0.386	square miles	mi^2
		VOLUME		
mL	milliliters	0.034	fluid ounces	fl oz
L	liters	0.264	gallons	gal
m^3	cubic meters	35.314	cubic feet	ft^3
m^3	cubic meters	1.307	cubic yards	yd^3
		MASS		
g	grams	0.035	ounces	oz
kg	kilograms	2.202	pounds	lb
Mg (or "t")	megagrams (or "metric ton")	1.103	short tons (2000 lb)	T
		TEMPERATURE (exact degrees)		
^oC	Celsius	1.8C+32	Fahrenheit	^oF
		ILLUMINATION		
lx	lux	0.0929	foot-candles	fc
cd/m^2	$candela/m^2$	0.2919	foot-Lamberts	fl
		FORCE and PRESSURE or STRESS		
N	newtons	0.225	poundforce	lbf
kPa	kilopascals	0.145	poundforce per square inch	lbf/in^2

* SI is the symbol for the International System of Units. Appropriate rounding should be made to co ply with Section 4 of ASTM E380.
(Revised March 2003)

TABLE OF CONTENTS

LIST OF FIGURES

LIST OF TABLES

EXECUTIVE SUMMARY

This study presents an integrated, nondestructive methodology for estimating cement content and as-built layer thickness in soil-cement bases and full-depth reclamation (FDR) with Portland cement. The approach utilizes ground penetrating radar (GPR) scans through laboratory experimentation to generate construction parameters that support quality control and performance verification.

Laboratory tests were conducted to establish relationships between electromagnetic (EM) properties and several cement moisture mixes. Soil-cement and FDR specimens were prepared with cement contents ranging from 0 to 9 percent and moisture contents spanning the dry, optimum, and wet sides of proctor compaction. Each specimen was monitored daily over an 8-day hydration period to record dielectric constant and electrical conductivity. The results captured the evolution of EM behavior during cement hydration as the dielectric constant decreased progressively when free water became chemically bound within the hydration products. The electrical conductivity declined sharply within 1 to 2 days because ionic mobility was restricted by the formation of calcium silicate hydrate (C-S-H) and ettringite phases.

Field surveys were performed using a 2 GHz air-coupled GPR system integrated with global positioning system (GPS) and a distance measuring instrument (DMI). Data were collected along one soil-cement site and five FDR construction sites. Spot percometer readings were taken along the constructed FDR sites, which also confirmed early age decline in the dielectric constant and electrical conductivity. Layer thickness was computed from two-way travel time, and electrical conductivity was derived from the GPR-measured dielectric constant. The field dielectric constant

and electrical conductivity were then mapped onto the laboratory calibration surfaces (i.e., contour plot) to estimate the cement content.

Analysis of the field data indicated that the stabilized layers were generally constructed within the target specification limits.

Estimated cement contents were mostly within the design range of 4–6 percent, although some localized deficiencies of 2.5–3.0 percent were observed. In addition, variations in moisture content, inconsistencies in cement mixing ratios, and differences in aggregate gradation with FDR depth were identified as construction-related factors contributing to localized performance instability within the stabilized layers. The layer thickness evaluation conformed to the design plans across most alignments. Core samples were taken at one site after construction to verify the layer thickness. Laboratory-prepared samples at the design mix (i.e., 6 percent cement, 10 percent moisture) achieved an average 7-day unconfined compressive strength of 324 psi, which did not exceed the Georgia Department of Transportation (GDOT) laboratory threshold of 450 psi. This strength reduction is likely attributable to changes in aggregate gradation during field FDR construction, where the coarse aggregate fraction decreased and the fine aggregate fraction increased, resulting in a weaker aggregate skeleton and lower overall compressive strength compared to the laboratory-prepared mix.

Key results include the following:

- The dielectric constant is governed primarily by cement hydration, conditioned by initial water content, and modulated by evaporation. Higher cement content accelerates hydration, converting more free water to bound water.

- The initial water content sets the baseline. Raising water content increases the starting dielectric constant and influences the minimum dielectric constant of the mix.
- Field GPR confirms the laboratory mechanism in the early curing days. Repeated surveys over the same alignment in the first few days after construction detect a progressive dielectric decrease consistent with hydration.
- Using GPR measurements of the dielectric constant and electrical conductivity, the cement content of the soil-cement and FDR sites was estimated and compared with the target cement content specified in the respective mix designs. The analysis revealed spatial variability in cement placement, with some sections exhibiting higher or lower cement content than intended. This non-uniform distribution is likely due to challenges in achieving consistent field placement and the lack of standardized guidelines for validating in situ cement content.
- In addition, at the FDR sites, aggregate gradation was observed to vary with depth, with some sections showing a reduction in the coarse aggregate fraction and an increase in the fine aggregate fraction relative to design requirements, potentially affecting strength and durability. For these reasons, stabilizing pavement subgrades based on cement content necessitates a comprehensive quality assurance/quality control framework that verifies not only cement content but also aggregate gradation, coarse aggregate fraction requirements, and other construction quality parameters.

CHAPTER 1. INTRODUCTION

BACKGROUND

Cement stabilization is commonly used in southern Georgia as a means of improving the strength of locally available fine-grained soils and preparing them for pavement construction. The use of these fine-grained soils is due to limited access to quarries for high-quality base materials.

The Georgia Department of Transportation (GDOT) relies on three types of cement stabilization: cement-stabilized subgrade (CSS), cement-treated base (CTB), and full-depth reclamation (FDR). Figure 1 shows the commonly used bases in each county in Georgia, including graded aggregate base (GAB) and asphaltic concrete (AC).

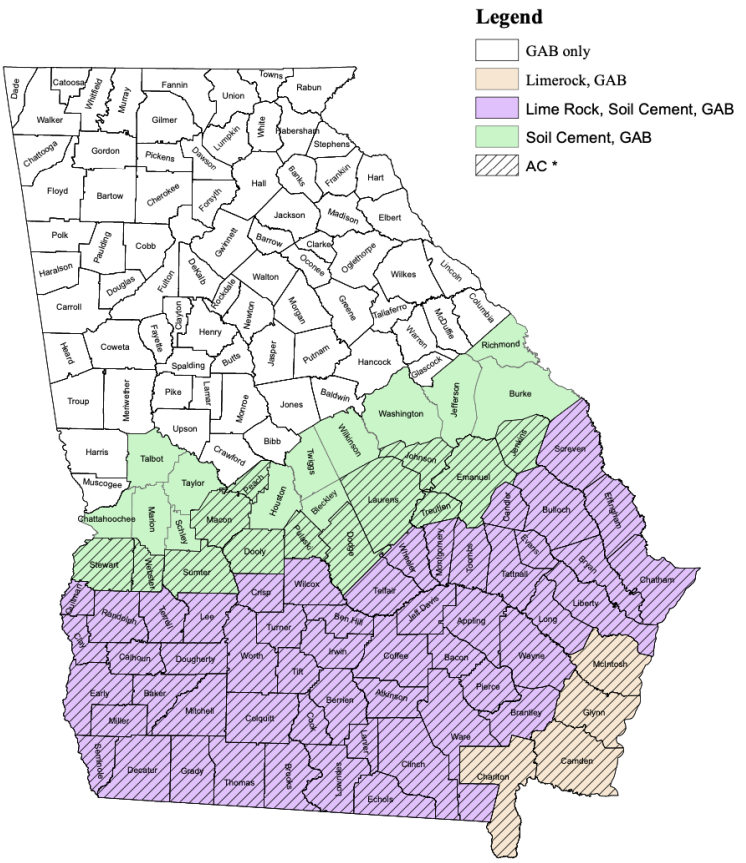

Figure 1. Map. Base uses in Georgia. (From: Georgia DOT Design Manual, https://www.dot.ga.gov/PartnerSmart/DesignManuals/GeotechnicalManual/4.5.16%20Base%20Uses%20in%20Georgia.pdf)

Cement-stabilized base and subgrade layers have emerged as a practical and cost-effective solution for road construction and rehabilitation across Georgia. Consequently, cement stabilization, particularly via FDR, offers an attractive alternative by recycling materials in place and reducing dependence on virgin aggregates. This in situ recycling method significantly reduces construction time, minimizes hauling and disposal requirements, and supports circular economy goals within transportation infrastructure.

PROBLEM STATEMENT

Flexible pavements over cement-stabilized soils may experience mild reflective cracking that originates from the shrinkage cracks on top of the stabilized layer. However, inadequate soil-cement construction, including thin stabilized layers, low compaction, deviations in cement content from the mix design, and rapid moisture loss, can greatly reduce the flexible pavement strength and overall life cycle.

The success of FDR and cement stabilization hinges critically on two interdependent parameters: cement content and layer thickness. These factors directly influence the mechanical behavior, durability, and service life of the pavement. Ensuring that the designed mix is followed on the construction site is critical. Figure 2 shows a spreader truck applying cement on an FDR construction site. Insufficient cement content may lead to inadequate strength and early-stage fatigue or shrinkage cracking, whereas excessive amounts could result in brittleness and poor long-term flexibility. Similarly, non-uniform or inaccurately estimated thickness can compromise load-bearing capacity, introduce stress concentrations, and undermine overall pavement performance.

Current practice verifies the cement content through destructive spot checks, which involves extracting cores and testing them in the laboratory. These methods are reliable at the point of sampling, but provide sparse spatial coverage and are time and labor intensive, disruptive to traffic, and vulnerable to sampling bias.

Figure 2. Photo. Cement application by a spreader truck on an FDR construction site.

RESEARCH MOTIVATION

Ground penetrating radar (GPR) offers the ability to rapidly scan large areas rapidly and infer subsurface characteristics based on reflected electromagnetic (EM) signals. Beyond conventional applications focused on thickness estimation and layer delineation, recent advances highlight the untapped potential of GPR to assess material properties through the dielectric constant and electrical conductivity.

OBJECTIVES

The main objectives of this project are to:

- Investigate a relationship among the dielectric constant, electrical conductivity, and cement content of cement-stabilized base/soil layers.
- Develop a methodology to assess the layer thickness variation of cement-stabilized base/soil layers.

- Lay groundwork to assess the percentage cement content and thickness variation of the FDR layer using GPR.

CHAPTER 2. LITERATURE REVIEW

MECHANISMS OF SOIL-CEMENT STABILIZATION

Cement stabilization improves the engineering properties of soils through a combination of physicochemical and microstructural mechanisms. During the initial stage, cation exchange associated with calcium ions and the subsequent compression of the diffuse double layer take place, especially in montmorillonite-rich clays, resulting in reduced repulsive forces between particles and enhanced soil stability. These expansive clays possess negatively charged surfaces that attract cations and form a water-laden diffuse double layer, contributing to high plasticity and swelling potential. When cement is introduced, divalent calcium ions (Ca^{2+}) replace weaker monovalent cations (e.g., Na^{+}), resulting in the collapse of the diffuse double layer. This leads to reduced interparticle spacing, enhanced particle packing, and improved soil workability and compaction (Little 1995, Sherwood 1993).

Simultaneously, hydration and cementitious bonding occur as the cement reacts with water, producing calcium silicate hydrates (C-S-H) and calcium aluminate hydrates (C-A-H), as displayed in figure 3. These compounds form rigid interparticle bonds, creating a cemented matrix that significantly increases unconfined compressive strength (UCS) and improves the structural integrity of the stabilized layer. In clay-rich soils, further strength development is achieved through pozzolanic reactions, where calcium hydroxide ($Ca(OH)_2$) released during hydration reacts with available silica and alumina in the soil. These secondary reactions produce additional C-S-H gel, enhancing long-term strength gain and durability (Consoli et al. 2007).

In addition to chemical transformations, microstructural reorganization takes place during cement treatment. The flocculation and agglomeration of fine particles result in a denser, more stable soil

fabric. This restructuring improves shear strength, reduces compressibility, and enhances resistance to long-term settlement and deformation. Together, these mechanisms form the basis of improved mechanical performance in cement-stabilized base and subgrade layers (Hausmann 1990, Mitchell and Soga 2005).

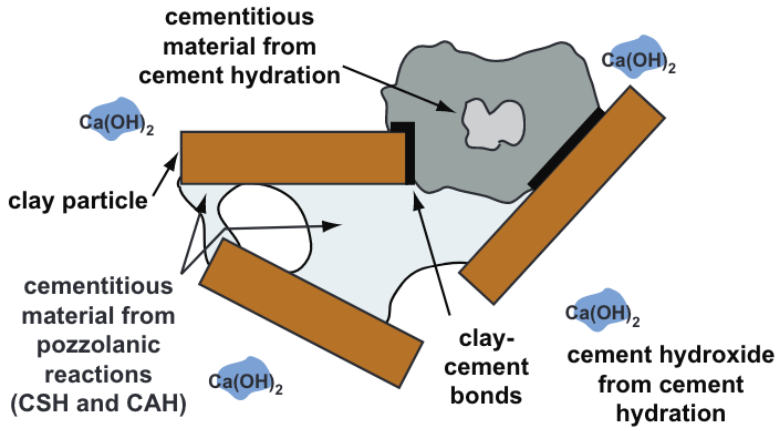

Figure 3. Image. Pozzolanic reaction (Halsted et al. 2008).

The primary goal of soil-cement stabilization is to remedy the accessible subgrade soils to sufficient strength and stiffness in order to carry the necessary design loads for the lifetime of the pavement. The use of cement in stabilizing soil should be carefully evaluated to meet the needs of the pavement without using too much cement. In concrete mix design, the water to cement (w/c) ratio is set to the minimum value requirement to meet the strength and durability requirements. The w/c ratio in concrete and soil-cement is simply the mass of the water divided by the mass of the cement. The standard equations for soil-cement mix designs are shown in equations 1, 2, and 3 (Portland Cement Association [PCA] 2020).

$$Cement\ Content, c\ (\%) = \frac{Weight\ of\ Cement}{Oven{-}Dry\ Weight\ of\ Soil} \times 100 \quad (1)$$

$$Water\ Content, w\ (\%) = \frac{Weight\ of\ Water\ in\ Mixture}{Oven{-}Dry\ Weight\ of\ Soil\ and\ Cement} \times 100 \quad (2)$$

$$Water\ to\ Cement\ Ratio, w/c = \frac{(1+c)\,w}{c} \quad (3)$$

Where:

c = % cement content

w = % water content

Case Study of Soil-Cement Stabilization

A review of five representative case studies highlights the proven versatility of cement stabilization as a ground improvement technique across varying soil types, structural demands, and environmental conditions. The effectiveness of stabilization was shown to depend largely on appropriate cement content, curing practices, and preconstruction evaluation.

In Iowa, a 4 percent cement application improved the performance of a lean to silty clay subgrade, with no cracking observed post-construction except in areas disturbed by underground utilities (Luhr et al. 2005). On California's SR-241 Toll Road, a similar 4 percent content achieved a 7-day UCS of 300 psi, resulting in long-term structural stability under high traffic volumes (Hartman 2016). At the Kentucky Airport taxiway, a 6 percent cement content to 16 inches depth significantly enhanced bearing capacity, with field performance validated under operational traffic (Fedrigi et al. 2020).

The Des Moines Airport project addressed sulfate-bearing silty clay, where preconstruction laboratory testing confirmed that 4 percent cement effectively mitigated expansion risks while tripling the untreated soil's strength. This emphasized the need for chemical compatibility analysis (Reeder et al. 2017). Lastly, a School Road project demonstrated that a 5 percent cement content

was sufficient to reduce both plasticity and expansion indices in sandy fat clay, confirming cement's role in shrink-swell mitigation (Barnes et al. 2012).

Across all case studies, cement contents ranging from 4 to 6 percent consistently enhanced the mechanical behavior of varied subgrade soils, including lean clays, silty clays, sandy fat clays, and sulfate-bearing materials. Notable improvements in UCS were recorded, with most projects achieving or exceeding the 300 psi benchmark within a 7-day curing window (Consoli et al. 2007). These strength gains translated into improved load-bearing capacity and overall pavement durability.

In problematic soils characterized by high plasticity or expansive behavior, cement stabilization effectively reduced both the plasticity index (PI) and expansion index (EI) to acceptable ranges for subgrade support. This demonstrated cement's dual role in improving strength and controlling volumetric instability (Sherwood 1993, Bell 1996).

Collectively, these case studies affirm that the successful application of soil-cement stabilization hinges on three interrelated factors:

1. Accurate soil characterization.
2. Appropriate cement contents selection.
3. Strict adherence to curing protocols.

FULL-DEPTH RECLAMATION AND THE ROLE OF CEMENT TYPE

FDR is an increasingly adopted pavement rehabilitation strategy that promotes sustainability, structural efficiency, and cost-effectiveness by recycling existing asphalt pavement and underlying base layers in place. Unlike conventional reconstruction methods that involve complete removal

and replacement of pavement materials, FDR employs a reclaimer machine to pulverize the deteriorated asphaltic surface and base, blend the reclaimed material uniformly, and incorporate stabilizing additive (i.e., Portland cement) to form a new, durable base course (Luhr et al. 2005, Hartman and Tazik 2016).

Modern reclaimers are engineered with precision control features, including automatic liquid additive control systems. These systems can adjust moisture content in real time based on variables such as cut width, milling depth, and machine travel speed (Fleming 2013, Wirtgen 2012). This automation ensures consistent water distribution, which is critical for achieving the desired hydration, compaction, and curing conditions. The pulverized mix is typically targeted to meet gradation criteria of 95 percent passing the 2-inch sieve, a specification that supports effective compaction and optimal interparticle contact for long-term stability.

The mechanism of strength gain in cement-stabilized FDR layers is driven by cement hydration reactions, which form binding compounds like C-S-H that fill voids and bond particles, thereby enhancing load-bearing capacity and moisture resistance. To balance strength and workability, Type I/II Portland cement is widely used due to its moderate heat of hydration and reliable curing profile. Nevertheless, sustainable alternatives such as Type IL (limestone blended cement) and binary cement blends containing slag or fly ash have shown promise in reducing embodied carbon while also mitigating risks of thermal cracking and improving long-term durability (Fedrigi et al. 2020, FHWA 2011). These blended cements exhibit slower heat release, prolonged setting time, and enhanced sulfate resistance, making them particularly beneficial in climates with aggressive environmental conditions. Moreover, curing conditions such as ambient temperature, relative humidity, and curing duration play a critical role in determining the success of stabilization.

GROUND PENETRATING RADAR FOR PAVEMENT EVALUATION

GPR has emerged as a key nondestructive testing (NDT) tool in geotechnical and pavement engineering and is widely adopted for subsurface characterization in pavement systems. Its advantages are high spatial resolution, rapid data acquisition, and the ability to operate at highway speed, which make it suitable for large-scale condition assessments and rehabilitation planning (Benedetto and Pajewski 2015, Daniels 2004).

In pavement applications, GPR is commonly used to estimate layer thickness, assess material uniformity, and detect moisture intrusions or voids. These functions are enabled by the radar's sensitivity to changes in dielectric properties at layer interfaces, which are influenced by factors such as material composition, moisture content, density, and degree of compaction (Daniels 2009). The dielectric constant (ε_r) measured from the reflected signals provides indirect but variable information about the physical and chemical states of stabilized materials.

As shown in the electromagnetic spectrum in Figure 4, as wave frequency increases, wavelength decreases. Consequently, the choice of antenna frequency significantly affects the quality and depth of data acquired. Low-frequency antennas (e.g., 200–400 MHz) offer deeper penetration but lower resolution, whereas high-frequency antennas (e.g., 1–2 GHz) yield high-resolution data ideal for detecting thin pavement layers, such as cement-stabilized bases. For this reason, 2 GHz air-coupled antennas are frequently employed in pavement studies where distinguishing shallow structural layers is critical.

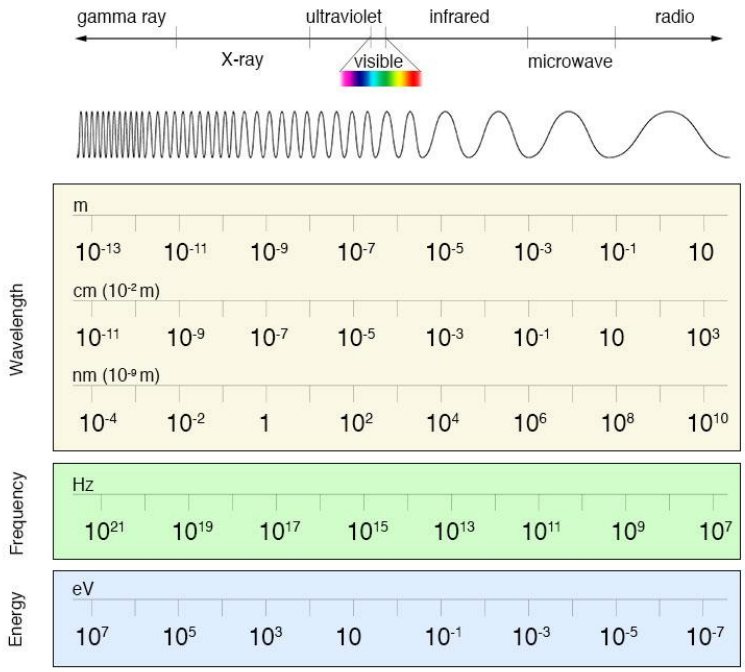

Figure 4. Image. Wavelength, Frequency, and Energy Representation of the Electromagnetic Spectrum. (Source: NASA, Electromagnetic Spectrum, https://imagine.gsfc.nasa.gov/science/toolbox/emspectrum2.html)

GPR Dielectric Constant Approach

A GPR system records the amplitudes from the reflected signal as well as their associated two-way travel times. The velocity of EM waves in many earth materials is estimated based on the wave regime approximation, which assumes the electrical conductivity is very small relative to the dielectric constant and frequency. Figure 5 shows typical reflections from the interface of pavements. Because the propagation time through the material is known, if the exact thickness of the material is also known, the velocity of the EM wave through the material can be calculated. This value can be imputed into equations 4, 5, and 6 to give the dielectric constant of the material:

$$\varepsilon_r = \left(\frac{c}{v}\right)^2 \quad (4)$$

Where:

ε_r = dielectric constant

c = speed of light in free space (3×10^8 m/s)

v = EM wave velocity (m/s)

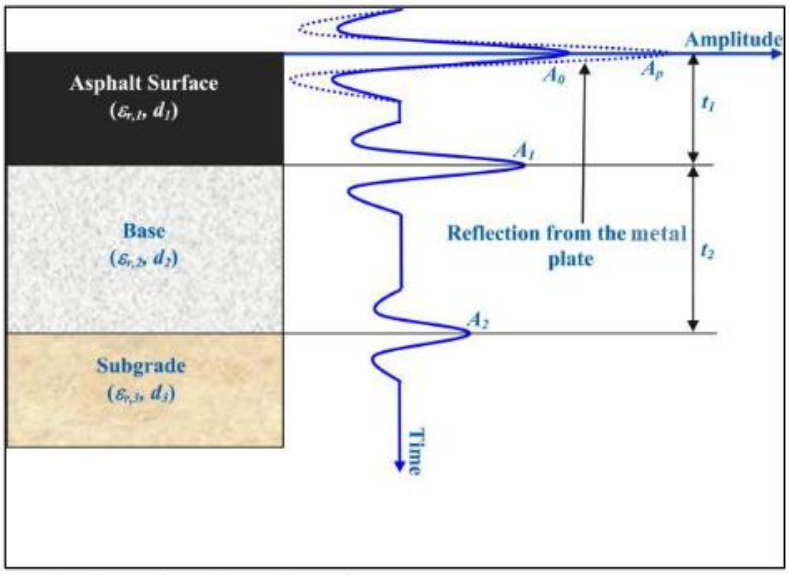

Figure 5. Image. Typical reflections from the interface of pavements (Leng and Al-Qadi 2014).

For most GPR surveys, the thickness of the layer being scanned is not known, and sometimes it is the parameter of interest. Thus, the following equation was created to estimate the dielectric constant based on the amplitude of the reflected wave from the surface relative to the amplitude of reflected wave from a perfect reflector (Al-Qadi and Lahouar 2005, Redman et al. 2002):

$$\varepsilon_r = \left(\frac{1+\frac{A_0}{A_m}}{1-\frac{A_0}{A_m}}\right)^2 \quad (5)$$

Where:

ε_r = dielectric constant

A_0 = amplitude reflection from the surface (V)

A_m = amplitude reflection from a metal plate larger than the GPR footprint (V)

The footprint of the air-coupled GPR can be calculated using the diameter of the first Fresnel zone (FZD) (Huisman et al. 2003, Tosti and Slob 2015).

$$FZD = \left(\frac{\lambda}{4} + 2h\lambda\right)^{\frac{1}{2}} \quad (6)$$

Where:

FZD = diameter of the first Fresnel zone (m)

λ = wavelength calculated at the GPR central frequency (m)

h = height of the antenna above the surface (m)

For most GPR air-coupled antennas, a 3 ft × 3 ft metal plate can provide the proper calibration amplitude. The metal plate calibration is performed before and after every GPR survey near the location being scanned to account for the variations in environmental changes.

RESEARCH GAPS

The dielectric constant and electrical conductivity are fundamental EM properties that offer valuable insights into the composition, moisture state, and hydration behavior of cement-stabilized materials. These parameters respond sensitively to variations in w/c ratio, material type, and curing progression, making them effective nondestructive indicators of microstructural evolution in reclaimed base layers (Pokkuluri 1998). The dielectric constant (ε_r), which quantifies a material's capacity to store electrical energy relative to vacuum permittivity (ε_0), is particularly influenced by the presence of free water; thus, higher w/c ratios typically yield elevated dielectric constant

values. Similarly, electrical conductivity reflects the availability of free ions in the pore structure and declines over time as hydration products restrict ionic mobility. Laboratory instruments such as the percometer enable rapid and nondestructive measurement of these properties in compacted geomaterials, with proven application in assessing volumetric moisture content, compaction uniformity, and ionic concentration (Humbolt 2017). Empirical studies have shown that both the dielectric constant and conductivity exhibit pronounced changes during early curing, which are markedly highest in the first 7 days due to abundant free water and ions, then stabilize as hydration progresses, making them reliable for evaluating cement content distribution and uniformity in cement-stabilized pavements (Pokkuluri 1998).

Recent research into cement stabilization and FDR reveals persistent gaps in translating controlled laboratory results into reliable, field-deployable tools for evaluating cement content. Whereas laboratory tests inform the mix design process, field performance often diverges due to uncontrolled curing environments, heterogeneous reclaimed base compositions, and moisture variability. Traditional methods such as coring, UCS, and falling weight deflectometer (FWD) testing are widely used but destructive, time-consuming, and spatially limited in their resolution.

A growing body of literature highlights the potential of EM properties, specifically the dielectric constant and electrical conductivity, for nondestructive evaluation of cement-stabilized layers. These parameters are sensitive to moisture content, cement hydration, and ionic concentration in pore fluids, making them promising indicators of cement content and curing progression. However, most existing studies either focus on laboratory-based dielectric probing or treat field GPR measurements primarily as tools for thickness estimation, without leveraging conductivity-related metrics for binder quantification (Loulizi et al. 2003, Kwon et al. 2020). In one notable laboratory-based study, Kim et al. (2016) demonstrated that both the dielectric constant and

electrical conductivity decreased with carbonation and strength loss in cement mortars. The experiment, conducted across 0.2- to 2-GHz frequencies using an open-ended coaxial probe, established strong correlations between EM properties, compressive strength, and hydration. However, the methodology was highly controlled and lacked scalability to GPR systems operating at fixed frequencies, limiting direct field applications.

Complementing this, Kargas et al. (2017) proposed a semi-empirical model linking dielectric response to soil-paste conductivity, incorporating moisture content and particle surface effects. Although this method offered a cost-effective alternative to extraction-based tests, it was not validated in field scenarios involving cementitious transformations, particularly those induced by hydration and curing in FDR bases. Kaya and Fang (1997) provided early foundational insights into the relationship between pore fluid characteristics and EM properties, demonstrating that moisture and ion concentration are key drivers of dielectric behavior in fine-grained soils. Although not focused on stabilized bases, their findings underpin the theoretical basis for later models.

More recently, Saha (2019) introduced a mechanistic-empirical model connecting dielectric properties to cement ion concentrations and evaporable water content in stabilized soils. Laboratory specimens were subjected to dielectric and conductivity testing alongside ASTM-based suction and moisture-density procedures. The study presented a theoretical expression for electrical conductivity based on GPR signal polarization, bridging EM physics with pavement sensing applications. Yet, despite this conceptual advance, real-time field deployment remains limited by the lack of calibration standards and contour translation methods.

Field-based studies further illustrate the complexity of applying dielectric–conductivity techniques under non-ideal conditions. For instance, Kwon et al. (2020) reported that early-stage FDR layers exhibited erratic GPR responses due to moisture-induced scattering and poor layer definition. This reinforced the need for dielectric calibration and moisture compensation when applying GPR in freshly reclaimed bases. By developing a predictive model that considered hydration rates, the dielectric constant, and conductivity, their study demonstrated the feasibility of estimating cement content.

Despite advancements in EM evaluation methods, a comprehensive framework that links laboratory-derived dielectric properties with field-based GPR data for cement content estimation in a cement-stabilized layer remains lacking. Key challenges include the absence of model validation under variable field conditions, lack of standardized calibration between laboratory and field data, and underutilization of GPR signal attenuation for conductivity estimation. Additionally, current methods fall short in converting EM data into spatially resolved cement content maps for field quality control. This study addresses these gaps by developing a field-calibrated dielectric–conductivity model that integrates GPR scans with percometer measurements, offering a transferable and nondestructive methodology for estimating cement content in FDR base layers.

CHAPTER 3. RESEARCH METHODOLOGY

METHODOLOGICAL FRAMEWORK

The methodological framework for this research is in three phases: laboratory investigations, field testing, and data analysis. The laboratory work involved carrying out various tests on the collected field samples, including the standard proctor test, percometer test, mix design module (MDM) test, sieve analysis, UCS test, and moisture content. Laboratory samples were prepared with the standard proctor mold, tested with the percometer and MDM, and then cured in a controlled chamber environment (20 ± 2°C, high relative humidity) according to GDOT. The MDM specimens were wrapped to seal in the moisture during the curing process. The samples were tested for 8 days, starting from the day they were molded. Figure 30 shows the soil cement dielectric constant hydration curve based on MDM measured from day 1 to day 7, with day 0 being the day the cores were made.

The field test involved the use of a 2-GHz air-coupled GPR and percometer to collect EM readings of the stabilized base layer. The dielectric constants measured from both percometer and GPR are compared, and a correction factor is applied to the dielectric constants measured from the GPR so that the dielectric constant measured using GPR match the dielectric constant measured using percometer. The data analysis involved interpreting the collected GPR data and the results of the laboratory percometer readings to estimate the cement content used on the construction site. This was also verified with the contractor's construction mix design.

This research is in two parts: soil-cement and FDR. These methodological frameworks are carried out in these two areas.

OVERVIEW OF SITE LOCATIONS

Soil-Cement Site

The soil-cement evaluation was conducted in Albany, Georgia, where conventional cement stabilization techniques were applied to improve subgrade performance. Figure 6 to Figure 8 illustrate key construction steps: Figure 6 shows the soil-cement mixing auger, figure 7 shows the spreading of soil-cement on-site, and figure 8 shows the compacted wet soil-cement layer.

Figure 6. Photo. Soil-cement mixing auger at the plant.

Figure 7. Photo. Jersey spreader, spreading the soil-cement on the construction site.

Figure 8. Photo. Compacted and wet soil-cement.

Full-Depth Reclamation

This study sampled five representative FDR sites across three counties in Georgia, representing various traffic and construction conditions. A summary of the FDR sites visited for this research is listed in table 1.

Four road projects (Log House Road, Brighton and Sagamore Lane, Old Covington Road, and Daniels Bridge) were designed at a uniform target depth of 10 inches with design cement contents of 6.0, 5.5, 5.3, and 4.8 percent, respectively. The sites cover functional classes with differing structural demands. The fifth site, Atlanta Motor Speedway, is a parking lot with intermittent traffic, designed with target depths of 6 and 8 inches and a cement content of 4.0 percent. Figure 9 to figure 11 illustrate the stabilized FDR bases at these sites: Figure 9 shows Atlanta Motor Speedway, figure 10 shows the GPR van scanning the Daniels Bridge Road base, and figure 11 shows the stabilized base at Old Covington Road.

Table 1. Summary of FDR sites visited.

Site No.	Name of Road	County	Date Visited	Target FDR Depth (inches)	Design Cement Content (%)	Traffic Class
1	Log House Road	Peachtree	Jul 17–20, 2025	10	6.0	Local/minor road collector (Neighborhood connector to schools/ parks)
2	Brighton and Sagamore Lane	Peachtree	Jun 2–6, 2025	10	5.5	Local residential street
3	Old Covington Road	Rockdale	Apr 1–3, 2025	10	5.3	Minor arterial corridor carrying traffic
4	Daniels Bridge Road	Rockdale	Mar 24–29, 2025	10	4.8	Residential collector with low moderate volumes
5	Atlanta Motor Speedway	Henry	Nov 8–14, 2024	6, 8	4.0	Private parking lot

Figure 9. Photo. Stabilized FDR base at Atlanta Motor Speedway.

Figure 10. Photo. GPR van scanning the stabilized FDR base at Daniels Bridge Road.

Figure 11. Photo. Stabilized FDR base at Old Covington Road.

CHAPTER 4. LABORATORY INVESTIGATION

SOIL-CEMENT LABWORK

Soil Physical and Chemical Properties

The soil used by the contractor performing cement stabilization was collected and utilized in the laboratory for creating soil-cement samples. The soil met the GDOT guidelines, and the result is shown in table 2. The soil was classified as GDOT IA1, which is medium-graded clayey sand. The soil can also be classified by the Unified Soil Classification System (USCS) as silty sand (SM).

Table 2. Soil physical and chemical analysis.

Item	Result	GDOT Spec Limit
GDT 6 Volume Change		
% Swell	5.2	—
% Shrink	0	—
Total Volume Change	5.2	18 Max
pH	6.30	4.0 Min
Sulfates	2.50 ppm	4000 ppm Max

Samples in the laboratory were created at a maximum dry density of 125 pcf and an optimum moisture content of 10 percent. This selection was based on the standard proctor test results for 5.5 percent cement. This was also the mix design that was used during field construction. Figure 12 shows the soil-cement standard proctor curve.

Cement was collected from the soil-cement plant during field testing for use in fabricating samples. This allowed for the minimization of variables when relating laboratory results to field measurements. The cement chemical and physical analysis was performed by the manufacturer, and the report for the batch used during construction is provided in table 3 and table 4.

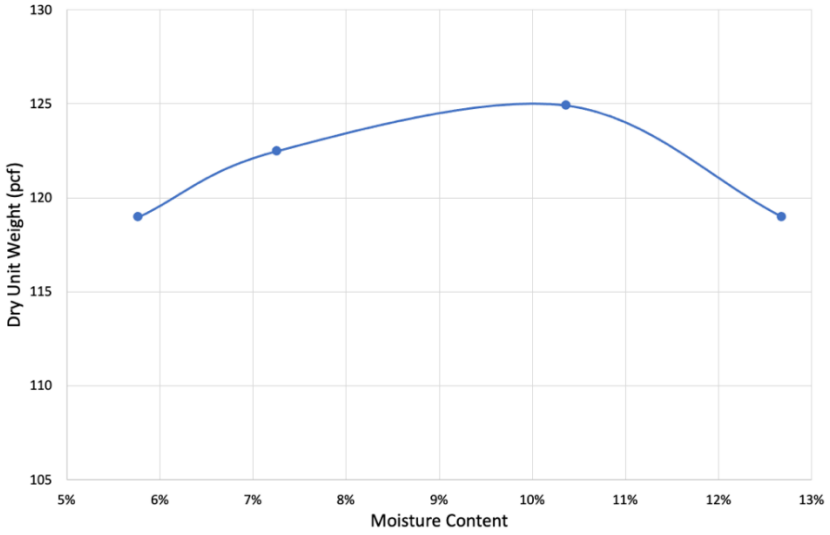

Figure 12. Graph. Soil-cement standard proctor curve.

Table 3. Chemical analysis of cement used during construction.

Item	Spec Limit (%)	PLC* Test Result
Rapid Method, X-Ray (C114)		
SiO_2	—	18.6
Al_2O_3	—	4.6
Fe_2O_3	—	3.2
CaO	—	63.2
MgO	—	0.8
SO_3	3.0 Max**	2.9
Loss on Ignition	10.0 Max	5.4
Insoluble Residue	—	0.42
Na_2O_{Eq} of Base Cement	—	0.35
CO_2	—	4.0
Limestone	5 to 15	7.7
$CaCO_3$ in Limestone	70 Min***	91
Inorganic Process Addition	—	1.9

* PLC = Portland Limestone Cement
** Max = Maximum
*** Min = Minimum

Table 4. Physical analysis of cement used during construction.

Item	Spec Limit	PLC* Test Result
Air Content of Mortar (%) (C185)	12 Max**	6.0
Blaine Fineness (m^2/kg) (C204)	—	474
Fineness, No. 325 Sieve (% Retained) (C430)	—	1.0
Density of Cement (g/cm^3) (C188)	—	3.08
Compressive Strength (psi [MPA]) (C109)		
1 Day	—	2210 [15.2]
3 Days	1890 [13.0] Min***	3890 [26.8]
7 Days	2900 [20.0] Min	4960 [34.2]
28 Days	3620 [25.0] Min	6440 [44.4]
Time of Setting (minutes)		
Vicat Initial (C191)	45 to 420	127
3 Days Heat of Hydration (kJ/kg) (C1702)	—	282
Mortar Bar Expansion (%) (C1038)	0.020 Max	0.009

* PLC =
** Max = Maxiumum
*** Min = Minimum

Mix Design Module Test

The Geophysical Survey Systems, Inc. (GSSI) MDM was selected for this study due to having an antenna with a 2-GHz central frequency, which matches the horn antenna used for the field testing. The MDM was created for asphalt testing to allow for the development of compaction data based on samples fabricated in a gyratory compactor. Therefore, samples scanned on the MDM have a diameter of at least 6 inches to cover the entire footprint of the antenna. The recommended height for asphalt samples is 75–120 mm.

The MDM is a standard GPR antenna that points upward and has a surface for placing a sample on top of it to allow for the entire signal to pass through it. Sample thicknesses are precisely measured and input into the software before scanning. The thickness of the sample is critical due to the dielectric constant being measured from the reflection of the signal through the entire sample.

Percometer Test

The percometer operates at a frequency of 40 MHz and processes the reflections in the internal equipment and gives a singular value for the dielectric constant and electrical conductivity.

The percometer is equipped with a 60 mm diameter surface probe. Samples were molded with soil passing the No. 4 sieve to eliminate the small percentage of larger particles present. The effective penetration depth of the percometer is 2–3 cm, depending on the material.

A limitation of the percometer is the low frequency of 40 MHz, which can result in a higher dielectric constant than the 2-GHz GPR antennas. This limitation was evaluated by scanning the MDM soil-cement samples with the percometer and comparing the results. Figure 29 shows a comparison of the dielectric constants measured using MDM and percometer. The dielectric constant measured with MDM would be similar to the dielectric from the 2-GHz GSSI antenna and will be lower than the dielectric constant measured using percomenter. The limitation of MDM is not having the capability to be usable in the field. The percometer was used in the field to collect dielectric constant and electrical conductivity values of the stabilized base.

Material Preparation

Twelve laboratory samples were tested to create a matrix and show the effect of different soil-cement mix designs on the dielectric constant and electrical conductivity. The mix design used by the contractor at the field testing was the same as sample 9. The other sample mix designs were based on typical cement contents used throughout southern Georgia. Table 5 shows the soil-cement sample mixes.

Table 5. Soil-cement sample mixes.

Sample	Water (%)	Cement (%)	Density (pcf)
1	6.0	0.0	132.5
2	8.0	0.0	135
3	10.0	0.0	137.7
4	6.0	3.0	132.5
5	8.0	3.0	135
6	10.0	3.0	137.5
7	6.0	5.5	132.5
8	8.0	5.5	135
9	10.0	5.5	137.7
10	6.0	8.0	132.5
11	8.0	8.0	135
12	10.0	8.0	137.7

A visual representation of the volumetric components of a standard mixture is shown in figure 13. The components of each sample mix design were weighed on a scale with a readability of 0.1 g.

Figure 13. Photo. Soil-cement sample mixture (5.5 percent cement and 10 percent water).

Soil-Cement Mixing

The soil was pulverized in a drum mixer to remove any large pieces of soil and allowed to pass through a No. 4 sieve. The soil was then dried to remove moisture and allow for accurate mixture

proportions. The soil-cement mixture proportions were then weighed out and placed in glass beakers.

The dry soil and cement were first combined in a large mixing bowl until a consistent color was seen. It was critical to fully combine the soil and cement to obtain the most homogeneous mixture possible. Next, water was added to the soil and cement, and then mixed until there were no lumps and an even color was achieved. Figure 14 shows the soil-cement final mixture.

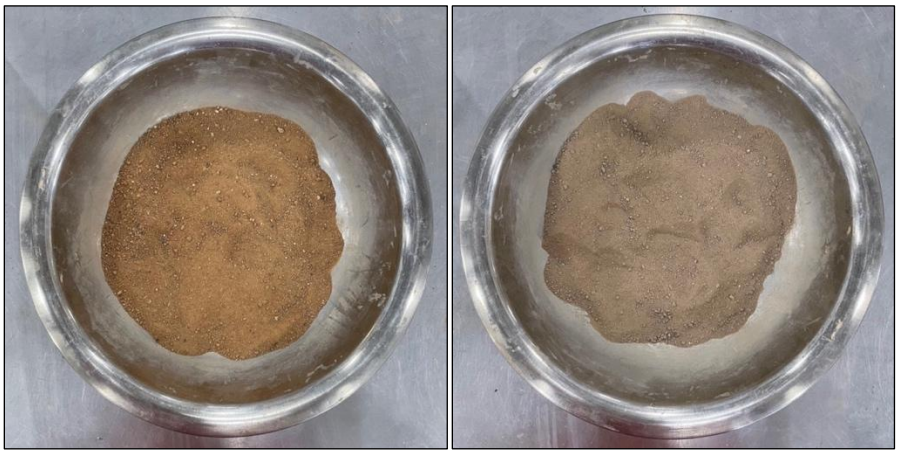

Figure 14. Photos. Soil and cement mixed (left) and soil-cement final mixture (right).

Percometer Scanning

The compacted soil-cement sample was then scanned on the top surface and the bottom surface (see figure 15). The top surface was where the sample was compacted and typically read lower values of dielectric constant and electrical conductivity than the bottom surface. The bottom surface was where the sample touches the base plate of the mold, so a larger moisture content was expected. Approximately eight percometer readings were taken on the top and bottom of the samples, which were then averaged.

Figure 15. Photos. Percometer scanning top (left) and bottom (right) of samples.

After the percometer readings were recorded, the soil-cement samples were immediately extruded from the mold by a sample jack and placed into plastic bags. The bags were tied shut and then weighed. This procedure allowed moisture to be sealed in the sample and prevented evaporation. A sample left exposed to air will decrease in dielectric constant much faster than in field conditions. The initial weight taken is an important reference point to monitor if the soil sample is losing moisture while curing.

MDM Scanning

The soil-cement samples were left in their curing bags (see figure 16) during the MDM scanning process. The plastic bag had little effect on the dielectric constant because the MDM measures the signal's time of flight as it travels through the entire sample.

To measure the dielectric constant using the MDM, the average thickness of each sample was recorded. The thickness is measured with a flat plate and dial gage to obtain a very accurate

thickness at many points on the sample (see figure 17). The thickness of the sample is the first input for the MDM software and can greatly affect the dielectric constant results.

Figure 16. Photo. Soil-cement MDM sample.

Figure 17. Photo. MDM sample thickness measurement.

FULL-DEPTH RECLAMATION LABWORK

Sample Preparation and Mix Design

Reclaimed base materials were obtained from every FDR construction site selected for evaluation. Upon collection, the materials were dried to remove residual moisture (see figure 18). The dried materials were then pulverized to break down agglomerates.

Gradation analysis was conducted in accordance with ASTM C136 (ASTM International 2019) and American Association of State Highway and Transportation Officials (AASHTO) T27 (2023), as shown in figure 19. The gradation curve for Brighton and Sagamore Lane FDR samples is shown in figure 20.

Figure 18. Photo. Collected field samples.

Figure 19. Photo. Sieve analysis.

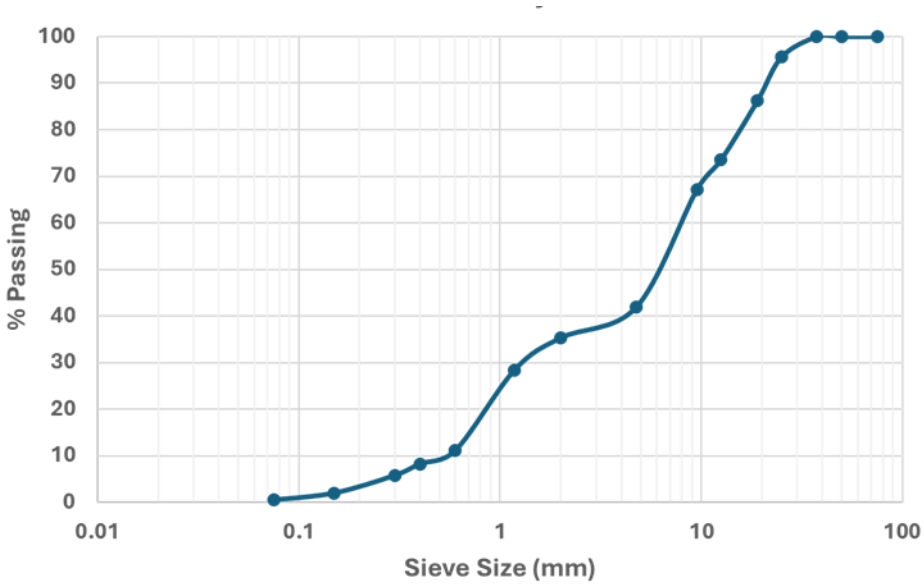

Figure 20. Graph. Gradation curve for Brighton and Sagamore Lane FDR samples.

FDR cement specimens were prepared with four target cement contents (0, 3, 6, and 9 percent) by dry weight of the aggregate reflecting typical field application rates for soil-cement stabilization. Each cement content level was mixed at three moisture conditions (4, 8, and 12 percent), representing dry, optimum, and wet-side conditions relative to Proctor compaction (see table 6).

Table 6. Soil-cement samples mix design.

Sample	Water (%)	Cement (%)	Density (pcf)
1	4	0	156.07
2	8	0	156.07
3	12	0	156.07
4	4	3	156.07
5	8	3	156.07
6	12	3	156.07
7	4	6	156.07
8	8	6	156.07
9	12	6	156.07
10	4	9	156.07
11	8	9	156.07
12	12	9	156.07

The mixing process involved thorough homogenization of cement and reclaimed base material, followed by the addition of water to achieve the desired moisture content. Samples were compacted into cylindrical molds (4-inch diameter × 4.6-inch height) using the Standard Proctor Method (ASTM D698; ASTM International 2021) to replicate field compaction energy. Specimens were immediately placed in a controlled laboratory environment (20 ±2°C and 95 percent relative humidity) to simulate curing conditions and mitigate moisture loss.

Measurement of the Dielectric Constant and Electrical Conductivity

The evolution of the dielectric constant and electrical conductivity was systematically monitored to evaluate the hydration and curing behavior of the FDR specimens. Measurements were taken using a precision dielectric probe (percometer) based on non-invasive EM principles. Each specimen was tested at scheduled time intervals from day 1 (initial compaction) through day 8, capturing the early-stage hydration period critical to cement stabilization performance.

FDR samples of the construction design mix were also molded (see figure 21) and crushed using the UCS test at 7 days (see figure 22).

Figure 21. Photo. Molded FDR cement sample.

Figure 22. Photo. Crushing the FDR sample during the UCS test.

CHAPTER 5. FIELD INVESTIGATION AND DATA ANALYSES

FIELD INVESTIGATION

Ground Penetrating Radar System

A GSSI 2-GHz horn antenna was selected for this study due to the high clarity of shallow subsurface layers and the aboveground positioning. The GPR van used for field testing was equipped with the GSSI distance measuring instrument (DMI) and a GPS antenna for location data.

The system settings shown in table 7 were set for the GPR data collection based on the manufacturer's recommendations. A custom filter was created and used for the time range and samples per second. This filter removes noise from the signal, providing more accurate results.

Table 7. GPR system characteristics used for testing.

GPR Antenna	Testing Parameters
GSSI Antenna Model	42000 S
Antenna Central Frequency	2 GHz
Pulse Width	0.5 ns
Antenna Height Above Surface	18 inches
GPR Software	
Time Range	18 ns
Samples Per Scan	1024

GPR Field Test at the Soil-Cement Site

The soil-cement site (see figure 23) was surveyed in four equal passes by the GPR van, with each pass spaced approximately 6 feet apart. This method allowed for the cement content to be estimated at most points in the new section. The first GPR scan was conducted immediately after the soil-

cement had been compacted and cut to grade. The dielectric constant change with time was monitored by conducting the same surveying procedure along the same paths for 5 days.

Figure 23. Photo. Soil-cement site.

After it was cut to grade, the soil-cement was primed to reduce evaporation of water from the surface and prevent the soil from scabbing and losing strength. When the prime coat was applied, the dielectric constant of the surface layer went up due to the addition of the thin, moist film. However, as the prime coat began to set and harden, the dielectric constant influence became negligible. Thus, it was recommended to not scan the surface when the prime coat was still very fresh.

FDR Investigation Using GPR

GPR field scanning was conducted across multiple FDR project sites in Georgia, including Atlanta Motor Speedway, Daniels Bridge Road, Old Covington Road, Brighton and Sagamore Lane, and

Log House Road. At each location, the survey vehicle traversed the stabilized road base, maintaining a consistent antenna height of approximately 20 inches above the pavement surface (see figure 24). GPR traces were recorded at 1024 samples per trace over a time range of 18 ns. After scanning the stabilized base with the GPR, the percometer was also used to collect the dielectric constant and electrical conductivity readings from the field (see figure 25). Core samples of the stabilized base layer were collected to ascertain the layer thickness of the construction (see figure 26). The locations where these core samples were collected were also tested with the GPR and percometer (see figure 27).

Figure 24. Photo. GPR scanning of the stabilized base.

Figure 25. Photo. Percometer scanning of the stabilized road base.

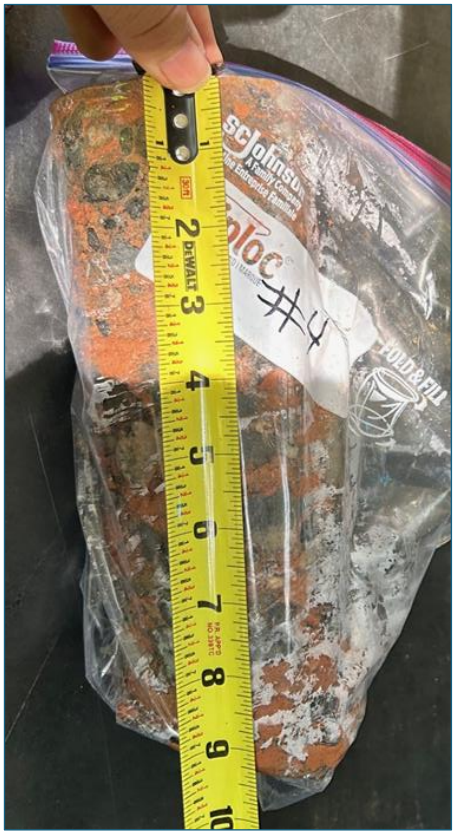

Figure 26. Photos. Collected core samples from the stabilized base.

Figure 27. Photo. GPR and percometer testing of the spots where cores were taken.

DATA ANALYSES AND PROCESSING

Obtaining Electrical Conductivity from the GPR Dielectric Constant

According to Crockford et al. (2021), construction variability and localized defects are significant contributors to reduced pavement service life. When evaluating subsurface conditions using EM methods such as GPR, the signal propagation angle becomes a critical factor influencing the accuracy of parameters like electrical conductivity. Analytical models typically consider two primary modes of wave propagation: normal incidence, where the radar wave impinges perpendicularly on the pavement surface, and non-normal incidence, where the wave strikes at an

oblique angle (see figure 28). The angle of incidence directly affects the reflection coefficients and attenuation behavior, thereby impacting how EM properties are interpreted.

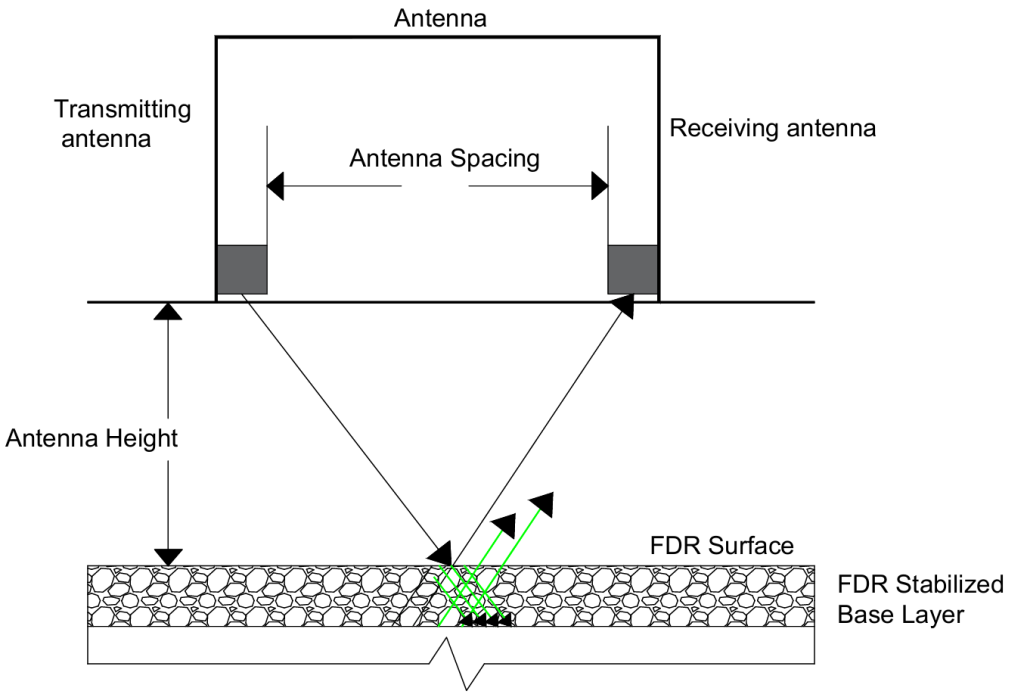

Figure 28. Image. Propagation of EM wave through cement-based material.

Postprocessing of the GPR signals was performed using RADAN 7 software (GSSI 2023) to derive the dielectric constant and antenna heights at each trace point. The electrical conductivity was derived following equations 7, 8, 9, 10, and 11.

The spacing between the transmitter and receiver antennas, along with the height of the antenna from the pavement surface, was used to calculate the angle of incidence.

Geometry and Angle of Incidence

The angle of incidence (θ) is set by the antenna standoff height and Tx-Rx spacing:

$$\theta = \tan^{-1}\left(\frac{\left(\frac{Antenna\ Spacing}{2}\right)}{Antenna\ Height}\right) \quad (7)$$

Where,

Antenna Spacing = the horizontal distance between the transmitter and receiver of the antenna (inches)

Antenna Height = the vertical separation between the antenna and the pavement surface during data collection (inches)

θ = the incident wave angle representing the angle formed between the transmitter radar wave path and a line normal to the pavement surface (radians)

$$b = \left(\frac{1}{\sin^2\theta}\right) \times \left(\frac{\varepsilon_1 \cos^2\theta}{\varepsilon_1}\right) \quad (8)$$

Where,

ε_1 = the GPR dielectric constant of the base layer

$$\text{term}_{(we)} = \frac{\varepsilon_1 \times 10^{-9}}{36\prod} \cdot 2 \cdot \prod F_{antenna} \quad (9)$$

Where,

$F_{antenna}$ = frequency of the antenna

$\text{term}_{(we)}$ = Frequency $\left(\frac{radians}{sec}\right)$ × Permittivity term

$$\text{term}_{(bn)} = b + \frac{1-2b}{n^2} \quad (10)$$

Where,

n = calculated constant for base course (derived from the percometer readings on the stabilized road base). This n-value varies for every construction site.

The electrical conductivity is then calculated using equation 11:

$$\sigma_{\textbf{positive}} = term_{\textbf{(we)}} \times \sqrt{\frac{n^4}{2b} \cdot term_{(bn)} \cdot \left(-1 + \sqrt{1 - \frac{4 \cdot (b-1)}{\frac{n^4}{2b} \cdot term_{(bn)}^{\,2}}}\right)} \quad (11)$$

Where,

σ_{positive} = conductivity, positive term

To estimate cement content from GPR data, the field-measured dielectric constant and derived electrical conductivity from the model were interpolated onto the laboratory-generated calibration surfaces. These surfaces, developed for different cement and moisture contents, relate dielectric and conductivity values to estimate the cement content.

CHAPTER 6. RESULTS AND DISCUSSION

SOIL-CEMENT RESULTS

Dielectric Constant and Electrical Conductivity Results

The dielectric constant and electrical conductivity for day 1 is shown in table 8. The bottom of the sample typically has higher value due to having a higher surface moisture content. However, a similar trend is observed for both sides.

Table 8. Dielectric constant and electrical conductivity from the percometer.

			Top of Sample		Bottom of Sample	
Sample	**Water (%)**	**Cement (%)**	**Dielectric Constant ε_r**	**Electrical Conductivity (µS/cm) σ**	**Dielectric Constant ε_r**	**Electrical Conductivity (µS/cm) σ**
1	6	0	7.1	7.5	9.2	14.3
2	8	0	9.3	19.5	12.4	82
3	10	0	14	69.8	14.8	90.3
4	6	3	6.6	29	9.7	36
5	8	3	8.3	46	12.5	293.3
6	10	3	14.5	259.4	16.1	556
7	6	5.5	8.9	32	9.7	23
8	8	5.5	11.4	99	13.2	239.6
9	10	5.5	13.9	330.3	14.3	630.2
10	6	8	8.8	42	11.0	114
11	8	8	10.1	0	12.2	195.75
12	10	8	15.4	489.8	15.4	721.2

The values of water content, cement content, dielectric constant, and electrical conductivity measured from the percometer will be used to generate surface chart models. Note that the variation in electrical conductivity is due to the variation in water content and this variation will occur with a constant cement content. The percometer operates at a central frequency of 40 MHz, whereas the MDM and GPR operate at a central frequency of 2 GHz. This leads to the percometer

having higher dielectric constants than the MDM. At higher moisture contents, the percometer and MDM become even farther apart. Figure 29 shows the percometer and MDM dielectric constant comparison for the day 1 samples.

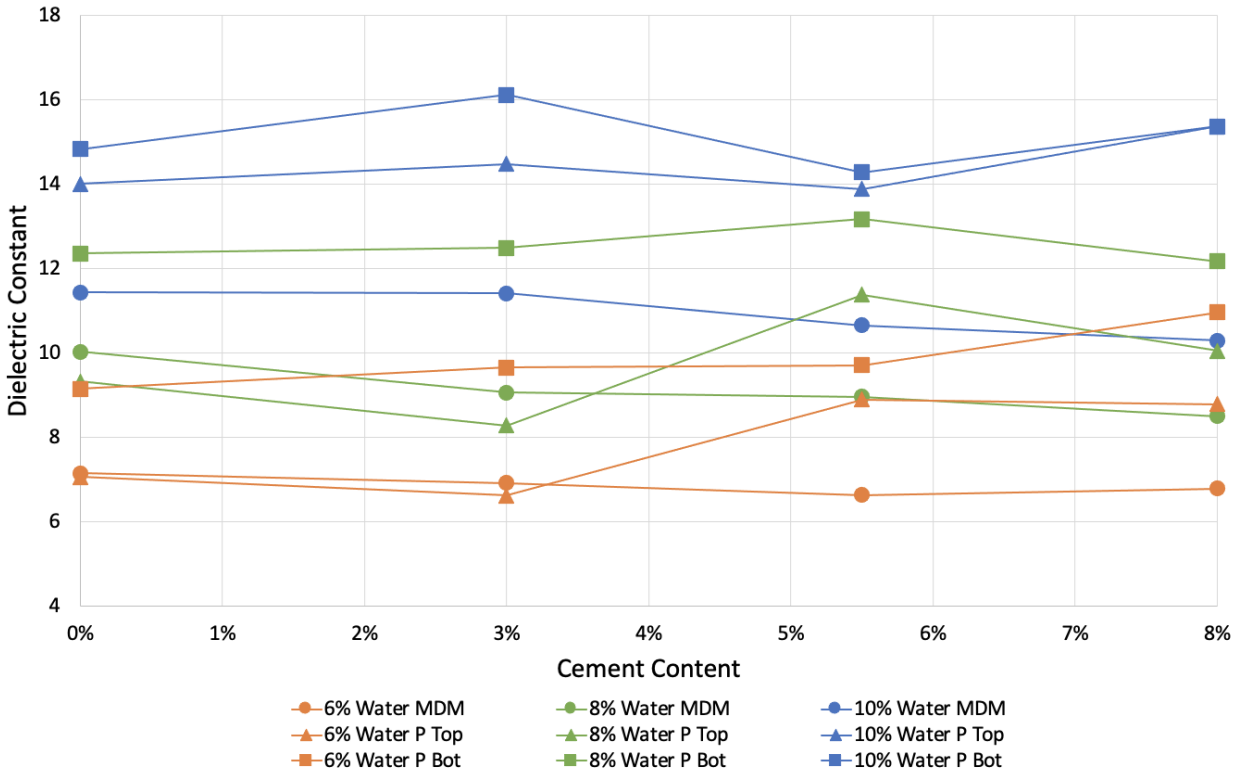

Figure 29. Graph. Percometer and MDM dielectric constant comparison for day 1 samples.

To account for this difference between the GPR and percometer, a correction factor can be applied based on the mix design of the sample. Although the dielectric constant is higher for the percometer, a similar trend for the 3D surfaces developed using the MDM could be found. Scanning samples with the percometer and the MDM allows for validation of similarity between the two devices.

Dielectric Constant Hydration Curves

The change in the dielectric constant with time was observed to be a function of cement content and water content. The samples were scanned for days 1, 2, 3, and 7 after fabrication. The resulting decrease in dielectric constant was a result of the free water being converted to chemically bound water. The effects of evaporation were minimal due to sealing the entire sample in a plastic bag. The samples stabilized with 8 percent cement exhibited a much greater decrease in dielectric constant than the samples with 6 and 3 percent cement. The effects of water content on the dielectric constant change were also observed. A sample with 10 percent water sustains a significantly higher dielectric constant than a sample with 8 percent water. This is because only so much free water can be converted into chemically bound water. Figure 30 shows the soil-cement dielectric constant hydration curve based on the MDM.

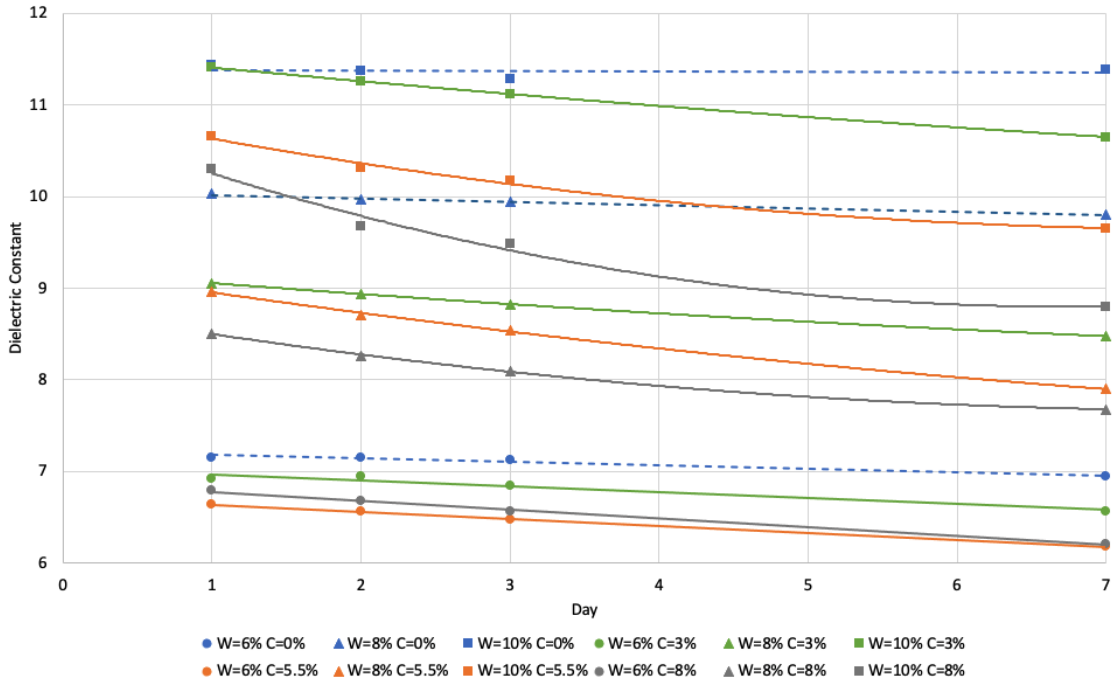

Figure 30. Graph. Soil-cement dielectric constant hydration curve based on the MDM.

The samples were scanned periodically following the first 7 days after fabrication to observe the continuous decrease in dielectric constant. A similar trend was observed for the dielectric constant of each mix design. However, the dielectric constant decreased at a slower rate for all samples. After 7 days, the cement hydration process had already formed approximately half of the total C-S-H that will be made. The strength gain was therefore a much slower process and took place until around day 28. Figure 31 shows the soil-cement dielectric constant hydration curve based on the MDM for 14 days after fabrication.

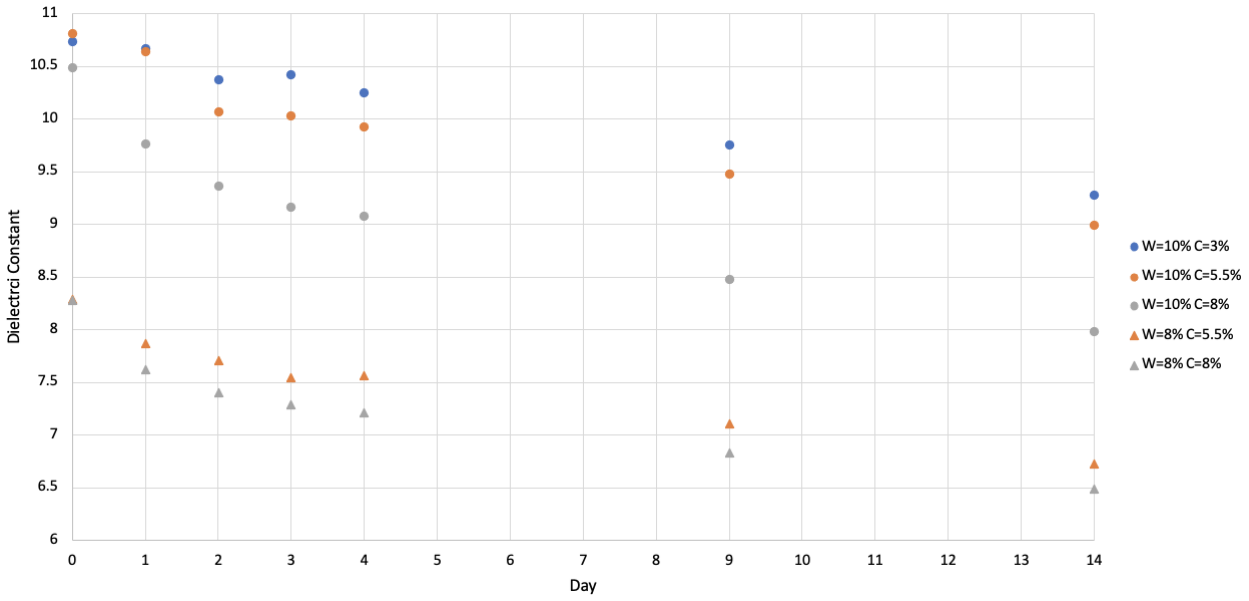

Figure 31. Graph. Soil-cement dielectric constant hydration curve based on the MDM for 14 days after fabrication.

Dielectric Constant Detection Surface

For the first few days after fabrication, a three-dimensional (3D) surface was developed to display the effects of varying mix design on the dielectric constant. Black dots represent data points derived from MDM scanning. The surface was created by using linear interpolation between the samples. This 3D surface was used for the cement detection model in which the GPR horn antenna

equation outputs a dielectric constant value, and then a horizontal slice was made along the *z* axis at that point. The output will then be a contour slice, which gives possible mix designs for that dielectric constant value.

For all 3D surfaces, a horizontal slice at a dielectric constant of 8.5 is shown. This plane produces the contours that show the possible cement and water content. The 3D surfaces for days 1, 2, 3, and 7 are shown with their respective contour lines in figure 32 to figure 39. The dielectric constant surfaces change with time greatly within the first 7 days. Therefore, it was critical to select the correct surface to match the day since the soil-cement construction for the section being scanned in the field.

Multiple contour lines around the selected slice value are also plotted to show how the 3D surface changes as the dielectric constant was increased or decreased. These lines were for visualization and were not the line currently being used for detecting the cement and water content.

The contour lines for each scanning day were kept on the contour plot. This allowed for understanding of how the dielectric constant surface changed with time. Four different solid contour lines can be seen, which were all found by slicing the respective days with a horizontal plane of dielectric constant equal to 8.5. The blue line represents day 1, and the purple line represents day 7. The points on the blue line all represent the initial mix designs capable of producing a dielectric constant of 8.5 on day 1. Similarly, the points on the purple line all represent the initial mix designs capable of producing a dielectric constant of 8.5 at day 7.

This method does not consider the effects of evaporation that will be experienced by soil-cement in the field. The dielectric constant decreased more for all mix designs in the field due to surface

evaporation. The advantage of looking at the dielectric constant change with time of samples with no evaporation is that the effects of only the cement hydration process can be investigated.

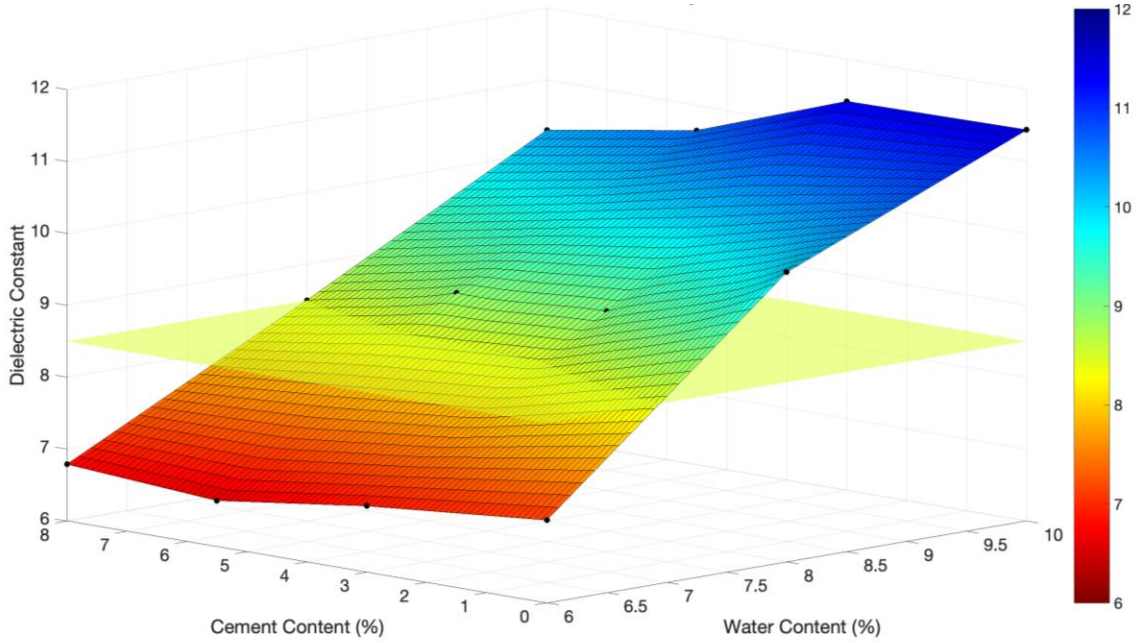

Figure 32. Graph. Day 1 dielectric constant surface.

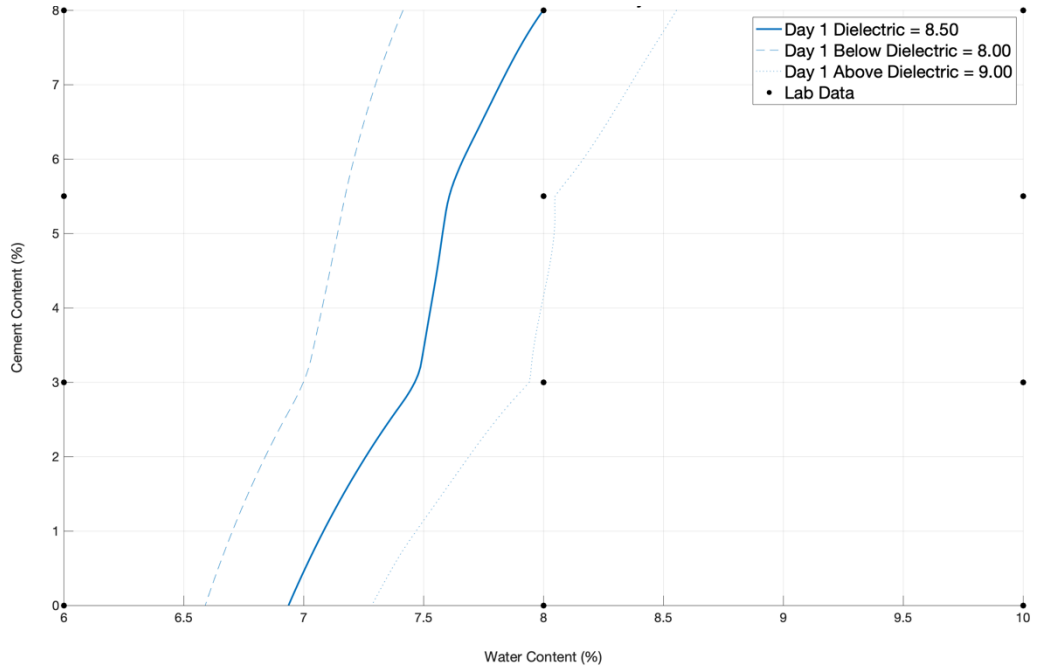

Figure 33. Graph. Day 1 dielectric constant surface contour line.

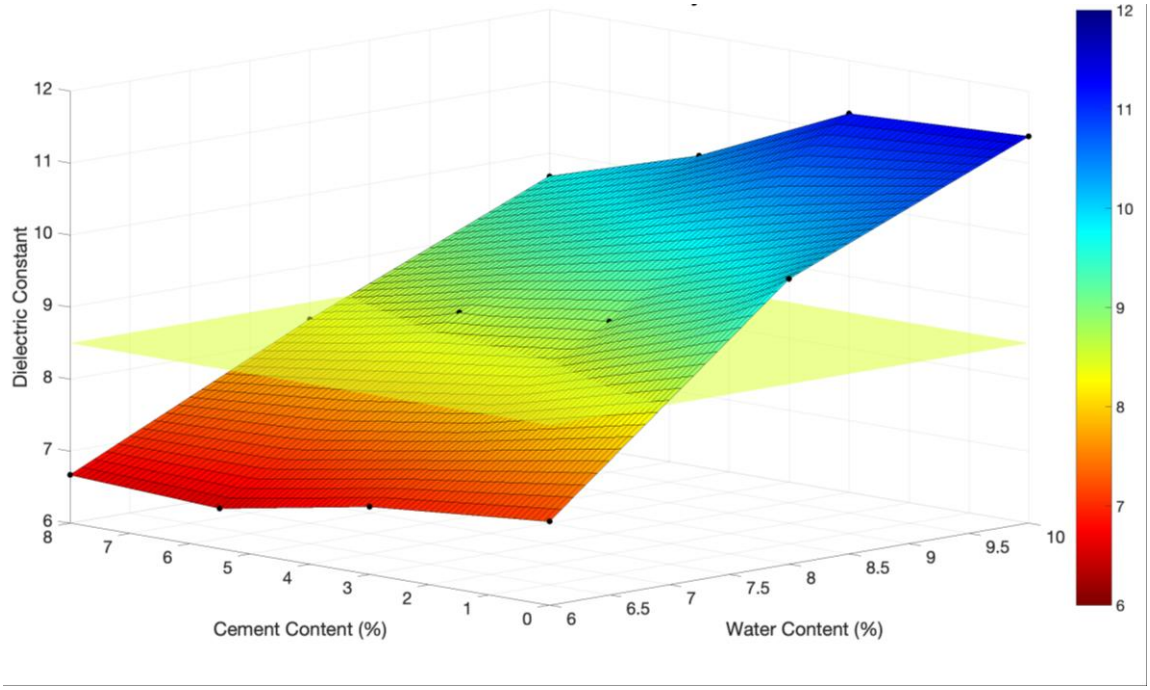

Figure 34. Graph. Day 2 dielectric constant surface.

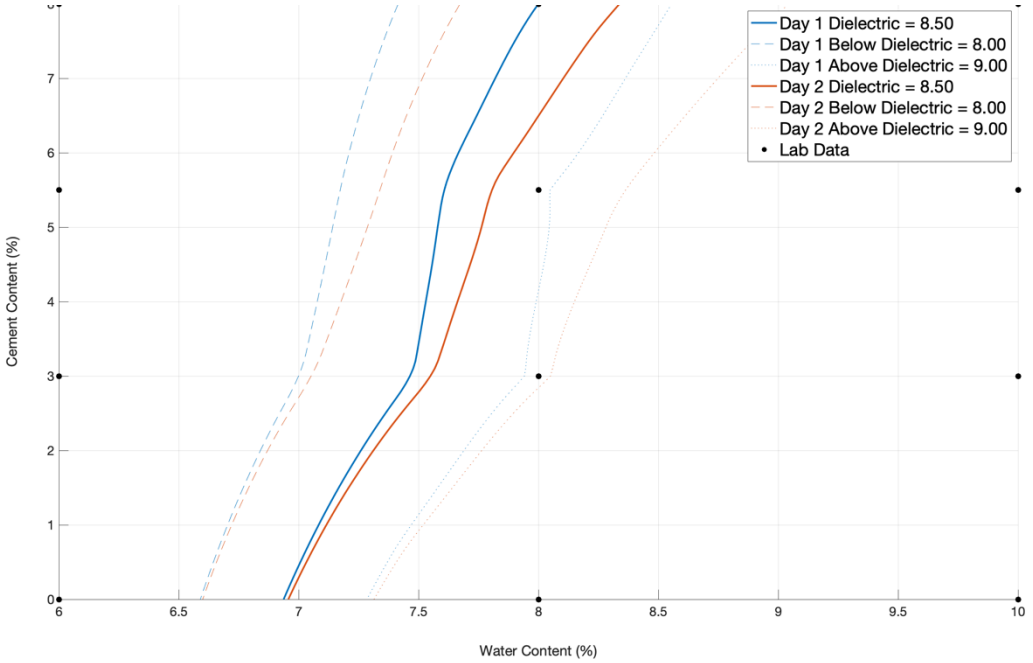

Figure 35. Graph. Day 2 dielectric constant surface contour line.

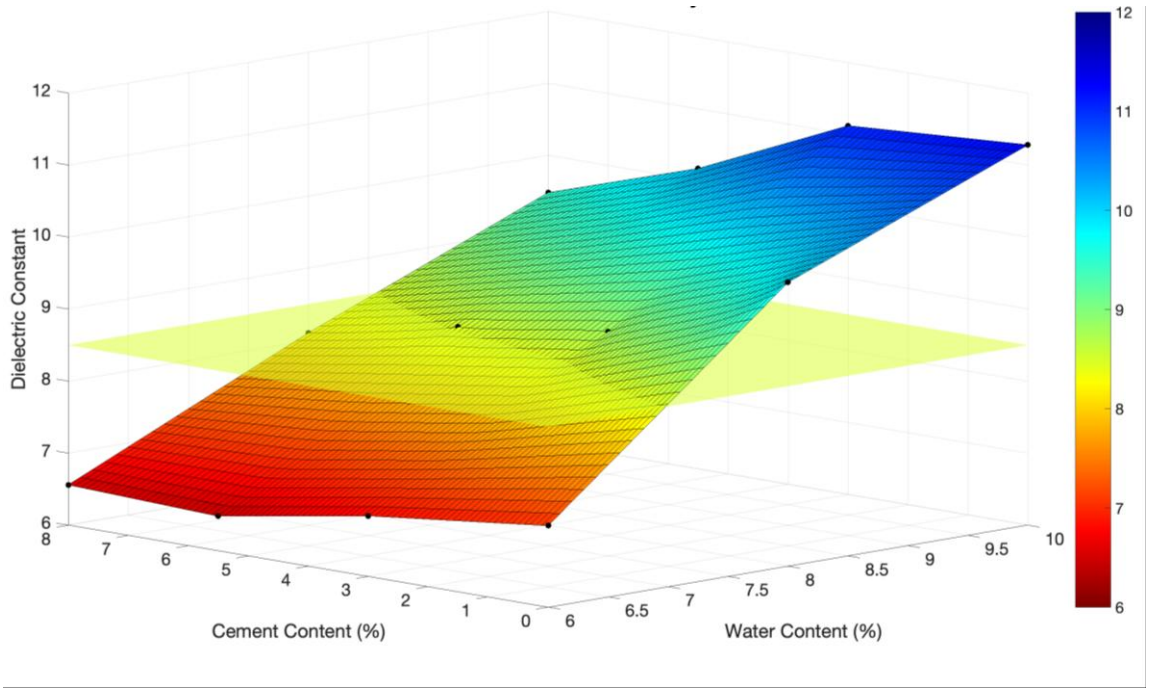

Figure 36. Graph. Day 3 dielectric constant surface.

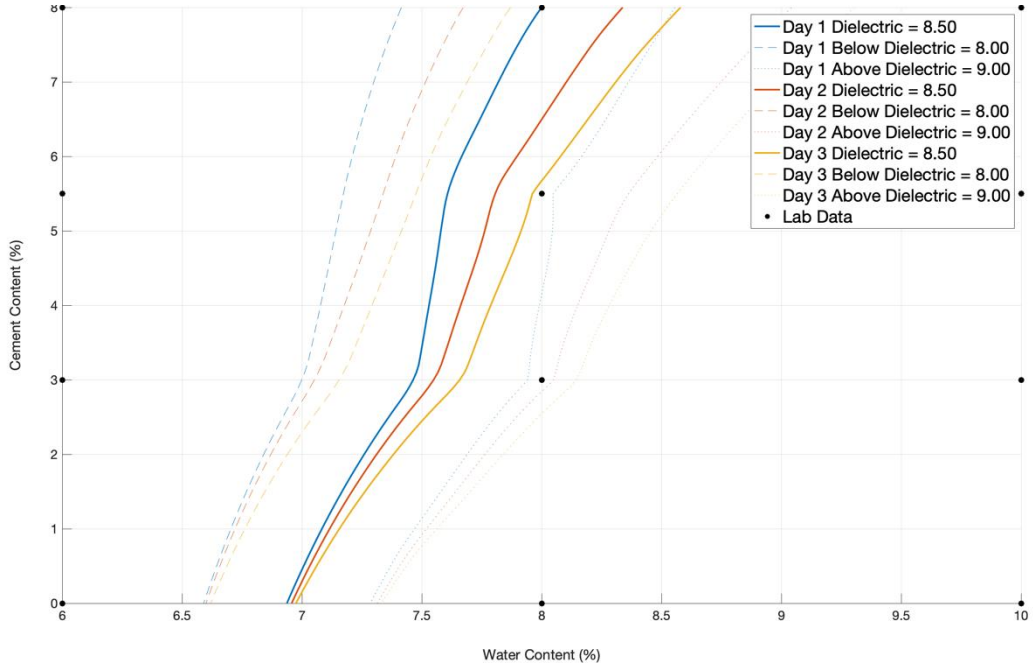

Figure 37. Graph. Day 3 dielectric constant surface contour line.

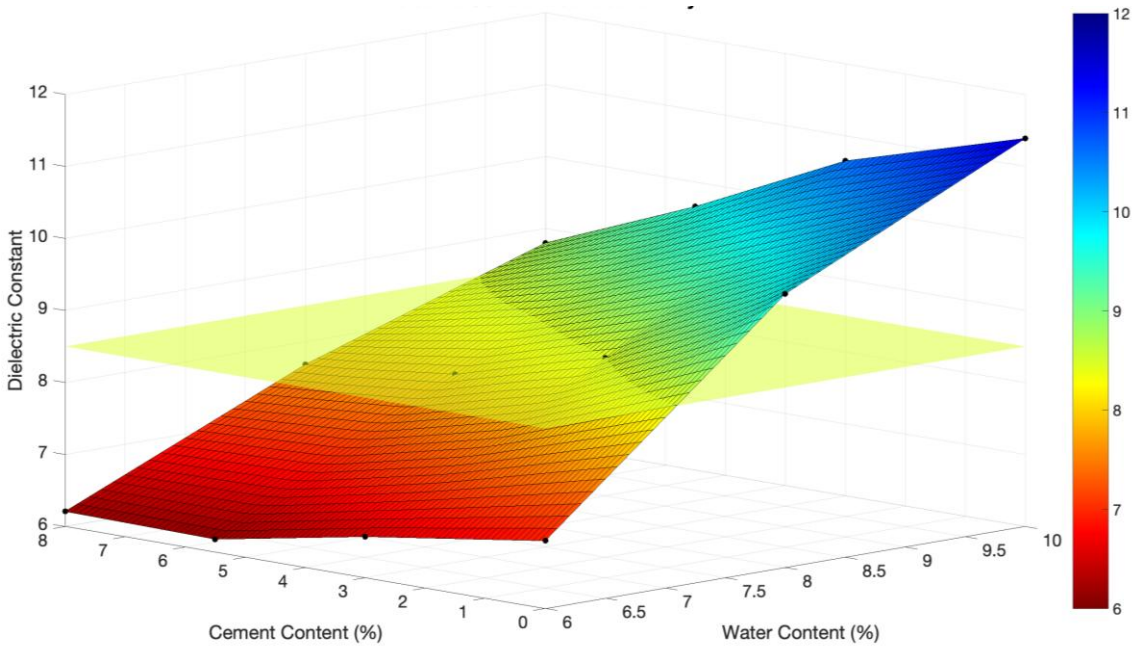

Figure 38. Graph. Day 7 dielectric constant surface.

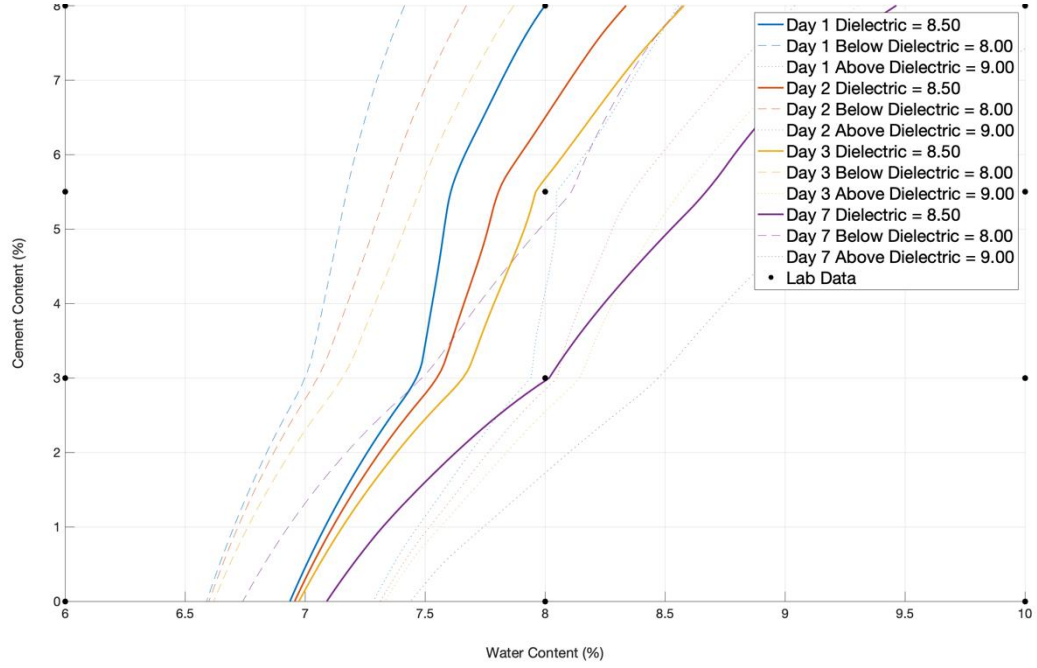

Figure 39. Graph. Day 7 dielectric constant surface contour line.

Electrical Conductivity Detection Surface

A 3D surface was developed to display the effects of varying mix designs on the electrical conductivity. Black dots represent data points derived from the percometer scanning the bottom of the samples. The surface was created by linear interpolating between the samples. This 3D surface was used for the cement detection model in which the GPR horn antenna equation outputs an electrical conductivity value, and then a horizontal slice was made along the *z* axis at that point. The output is a contour slice, which gives possible mix designs for that electrical conductivity value.

The electrical conductivity of the soil-cement samples was scanned for the first day after fabrication, and then the samples were scanned only by the MDM. The electrical conductivity changed with time, but the change was not as drastic as the dielectric constant from the GPR measurements.

A horizontal slice at an electrical conductivity of 300 μS/cm is shown on the 3D surface. The resulting contour slice is also shown in figure 40 and figure 41. Similar to the dielectric constant contour lines, the contour lines for an electrical conductivity slightly above and below the target slice are shown for visualization. The points along the solid blue contour line all represent the initial mix designs capable of producing an electrical conductivity of 300 μS/cm at day 1.

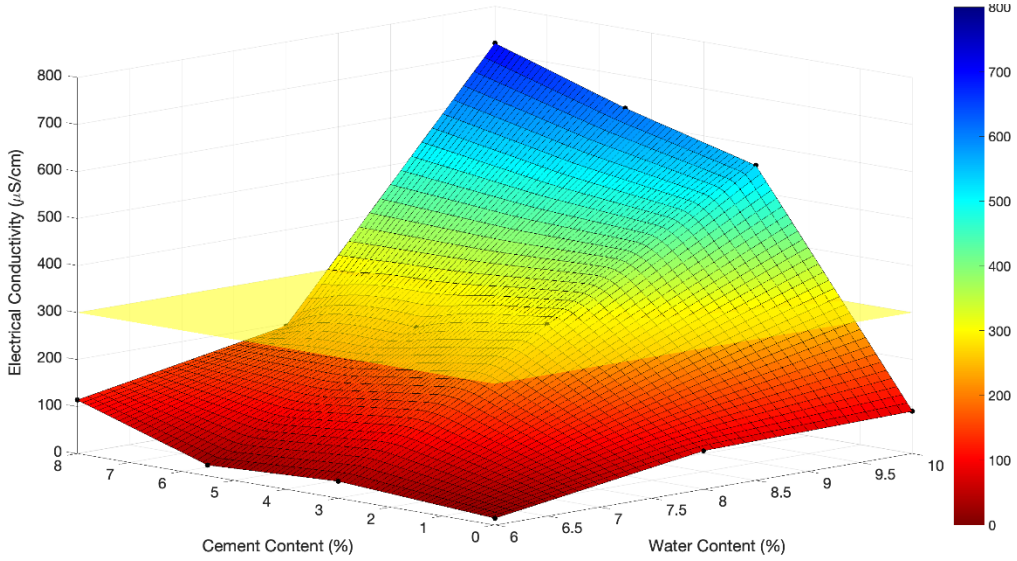

Figure 40. Graph. Day 1 electrical conductivity surface.

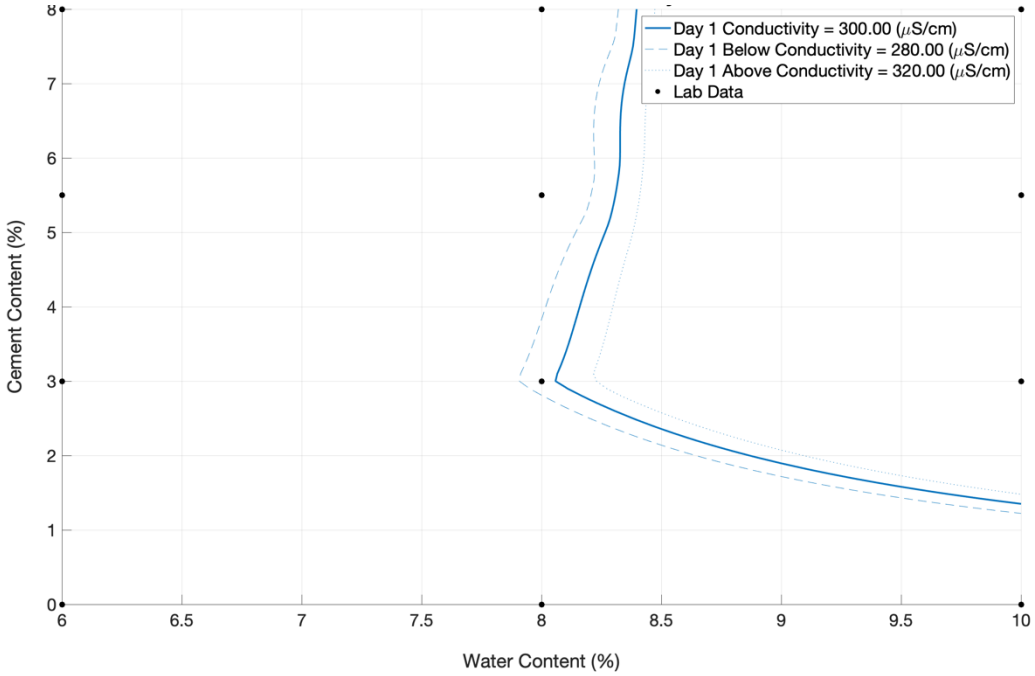

Figure 41. Graph. Day 1 electrical conductivity contour line.

Cement Content Detection Model

The cement and water content for the initial mix design can be estimated by performing a GPR survey within the first few days of construction. The dielectric constant and electrical conductivity

are determined at every scan distance interval the GPR van travels. The 3D surfaces developed for the specific soil being used can then be used for their respective day. The dielectric reading from the field was input into the model to find the cement and water content along that contour plane. The same step was performed for the electrical conductivity. The intersection was then found between the dielectric constant and electrical conductivity planes. This intersection point is the cement and water content for the specific point in the field that was placed on the day of construction.

The contour lines occasionally intersect more than once, resulting in multiple mix design predictions. To determine which intersection point is accurate, the GPR van should scan the same path for multiple days. The hydration rate can then be estimated based on the dielectric constant hydration curves for the respective days scanned. For figure 42, a soil with approximately 7.8 percent water and 2.5 percent cement will experience much less dielectric constant change with time than a soil sample with 8 percent water and 5.5 percent cement. Therefore, the correct intersection point can be selected based on the contour slice intersection and dielectric constant change.

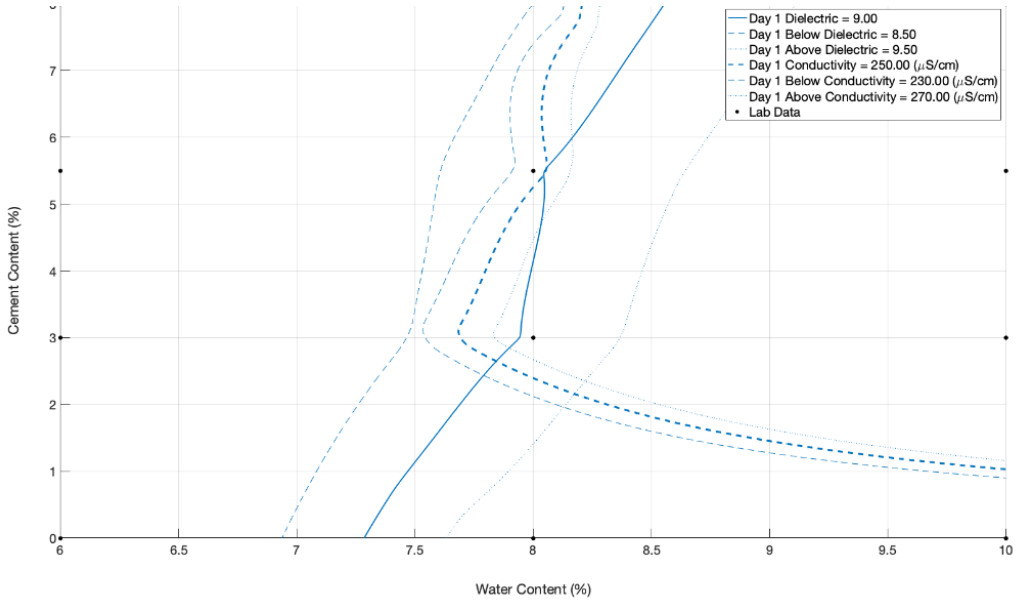

Figure 42. Graph. Dielectric constant and electrical conductivity contour line intersection.

Field Testing Results

The dielectric constant decrease with time was detected for the soil-cement layer from scanning the same path for 4 days after construction, as shown by the results in figure 43 and figure 44. Figures 43 and 44 present the survey results from the first and second passes, respectively, illustrating the variation in dielectric properties along each path which is approximately 6 feet apart. The decrease in dielectric constant was close for many of the locations along the path. However, there are a few areas where the hydration rate was likely higher due to a higher cement content.

The blue dots from the field testing are a result of surface water on the cement-stabilized layer. The surface water had a very high dielectric constant of around 81, so even a thin layer led to a large spike. To accurately capture the dielectric constant of the soil-cement, points with a dielectric constant above 10 were not considered in the running average analysis.

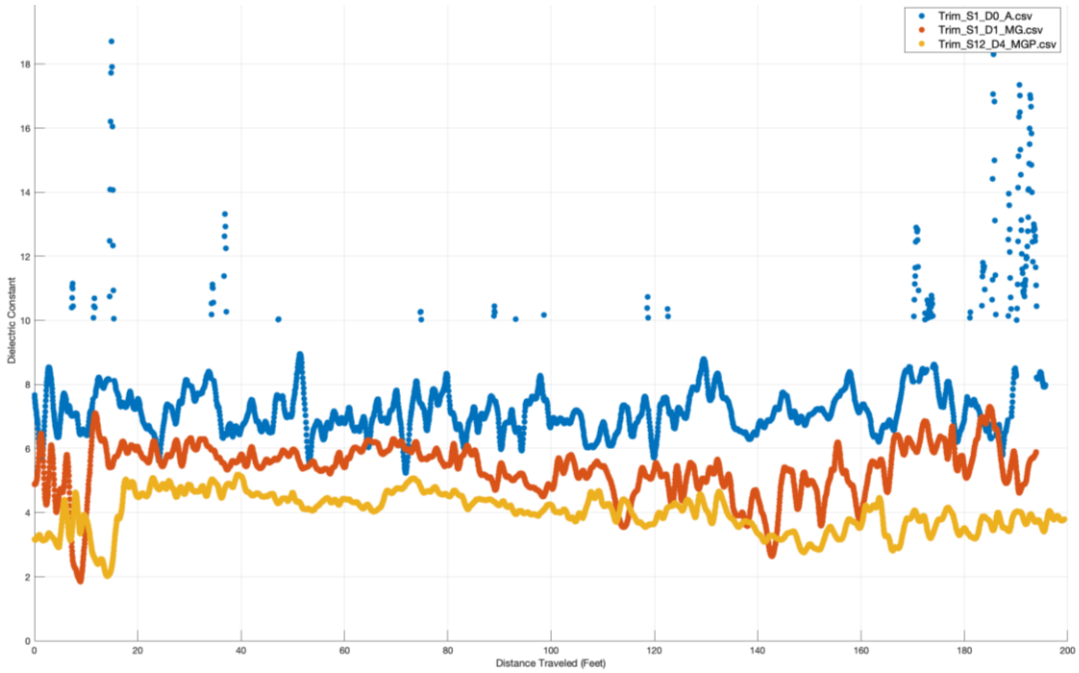

Figure 43. Graph. Albany soil-cement site, first path.

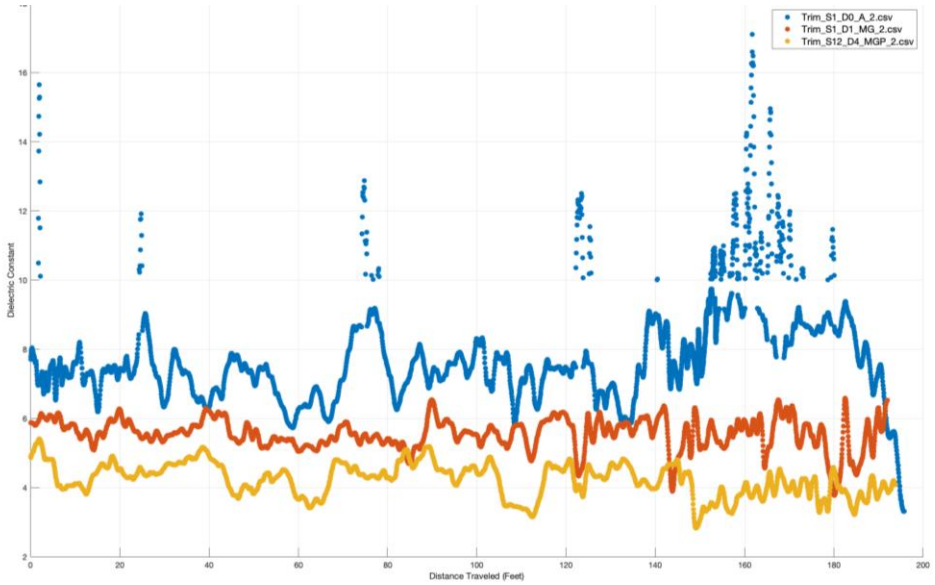

Figure 44. Graph. Albany soil-cement site, second path.

The purpose of this initial field testing was to identify the dielectric constant change with time. The cement and water content were not predicted using the surface intersection method due to the model not being developed at the time. The results of this site visit are still important to understand

the field conditions of soil-cement and the effects that surface evaporation has on the change with time. The estimated cement content for the soil-cement site is shown in figure 45. The estimated cement content began at the onset within the 4.5–5.0 percent range for the first 100 ft and then ranged between 5.8 and 6.3 percent before settling to a stable plateau between 5.1 and 5.4 beyond 300 ft. Generally, the estimated cement content fell between 4.5 and 6.0 percent of cement content, which aligns with the design mix.

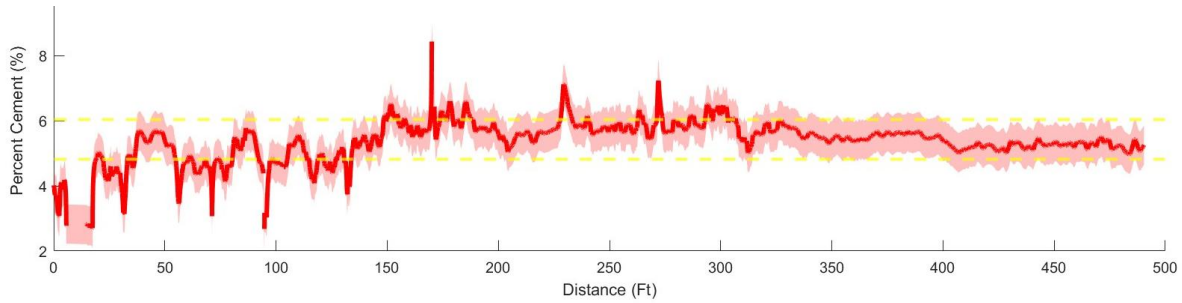

Figure 45. Graph. Estimated cement content for soil-cement site.

FULL-DEPTH RECLAMATION RESULTS

Three FDR reclaimed base materials with depths of 6, 8, and 10 inches were sampled from two FDR sites. The 6- and 8-inch samples were collected at the Atlanta Motor Speedway, and the 10-inch sample was taken from Daniels Bridge Road. Figure 46 shows the gradation curves of the 6-, 8-, and 10-inch FDR samples.

The gradation analysis revealed a depth-dependent variation in particle size distribution. At the coarse aggregate level, all three depths exhibited nearly complete passage, confirming the absence of oversized materials. However, the coarse aggregate fraction and fine aggregate fraction varied with depth. Specifically, the 6-inch sample showed lower percent passing at the 25 mm sieve compared to the 10-inch sample, indicating a higher coarse aggregate fraction at shallower depths. Additionally, the No. 4 sieve (2.0 mm) passing (fine aggregate fraction) was less than 10 percent

for the 6-inch sample but increased significantly to 36 percent for the 10-inch sample. In the intermediate fraction, a clear trend of increasing fineness with depth was observed; for example, percent passing at the 12.5 mm sieve increased from 45 percent in the 6-inch sample to 73.5 percent in the 10-inch sample.

This trend can be attributed to the incorporation of subgrade soils into the FDR mix as depth increases, which leads to an increase in the fine aggregate fraction and subsequently affects the hydration reaction of cementitious stabilization and the UCS. Therefore, it is recommended to monitor the particle size distribution and coarse/fine aggregate fractions when determining FDR depth and to verify compliance with design specifications through post-construction quality assurance/quality control (QA/QC) procedures.

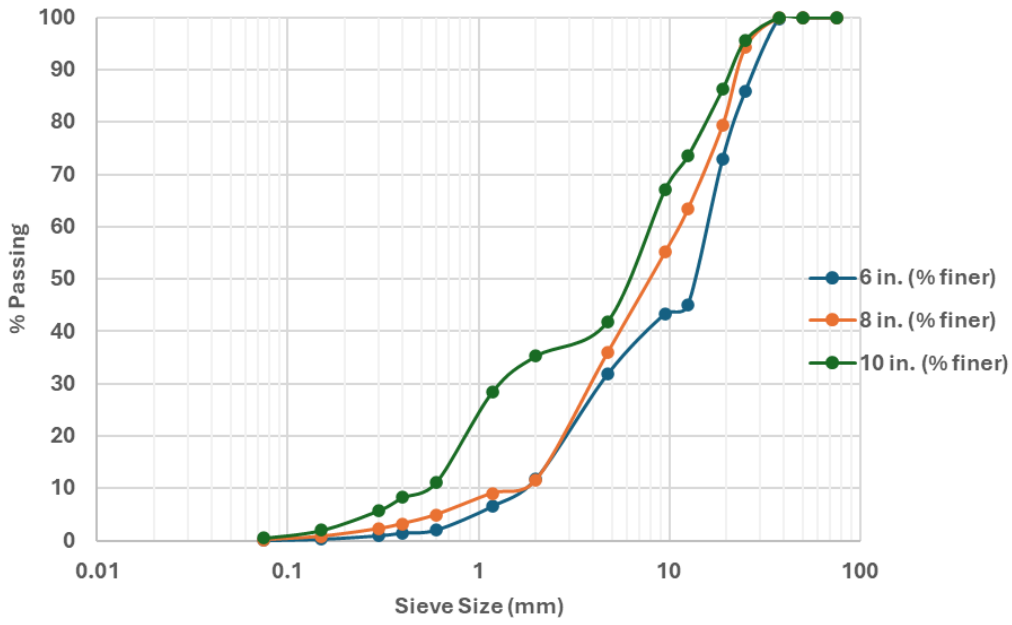

Figure 46. Graph. Gradation curve of 6-, 8-, and 10-inch FDR samples.

Log House Road FDR Site

A moisture content test was carried out on the FDR samples collected in the laboratory. The average moisture content for the reclaimed sample was 9.23 percent. Table 9 shows the results of the moisture content test.

Table 9. Sample moisture content.

	Specimen #1	Specimen #2	Specimen #3
Wet (g)	876.0	498.0	1352.5
Dry (g)	803.0	454.0	1242.0
Wet-dry (g)	73.0	44.0	110.5
Water content (%)	9.1	9.7	8.9
Average (%)	**9.2**		

Laboratory results for the dielectric constant and electrical conductivity showed a clear monotonic reduction with curing time at every cement moisture combination, tracking the transition from a free water ionic state on day 1 to a hydration-controlled, low-loss matrix by day 8.

Two features were evident, First, most of the dielectric constant drop occurred within the first 3–4 days, as free water was consumed and immobilized in C-S-H/aluminate ferrite trisulfate (C-S-H/AFT; i.e., ettringite) gels and capillary continuity broke down, indicating microstructural stabilization. Second, at a given moisture content, cement content influenced the final (end-state) dielectric constant. While differences were observed at 4% and 8% moisture, the dielectric constant reached a similar minimum at 12% moisture, suggesting that this corresponds to an effective paste volume that optimizes pore refinement. The 3 percent cement with 12 percent moisture remained comparatively high on day 8, which is consistent with insufficient cement to redistribute the larger water inventory within the sample. Conversely, the 9 percent cement did not

finish lower than the 6 percent cement on day 8. The 3D dielectric constant contour surface for day 1 is shown in figure 47.

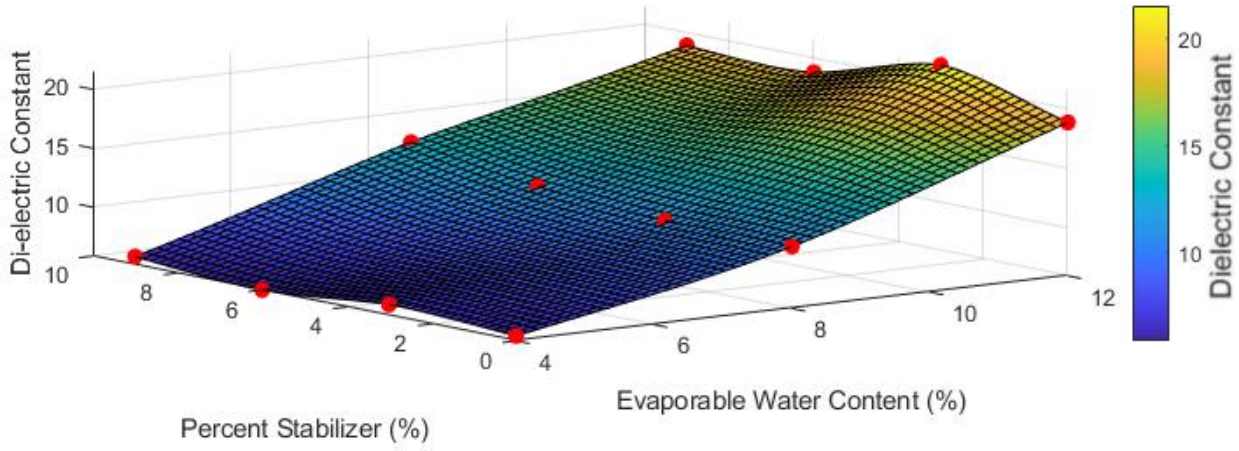

Figure 47. Graph. 3D contour plot surface for day 1 dielectric constant results.

The laboratory electrical conductivity results showed high values on day 1 in wet states and a steep decline by day 2, with negligible conductivity from day 3 onward. At 12 percent moisture content, electrical conductivity was highest, whereas at 8 percent only modest values appeared. This pattern indicates free pore water and mobile ions at the bottom of the specimen. The 3D electrical conductivity surface for day 1 is shown in figure 48.

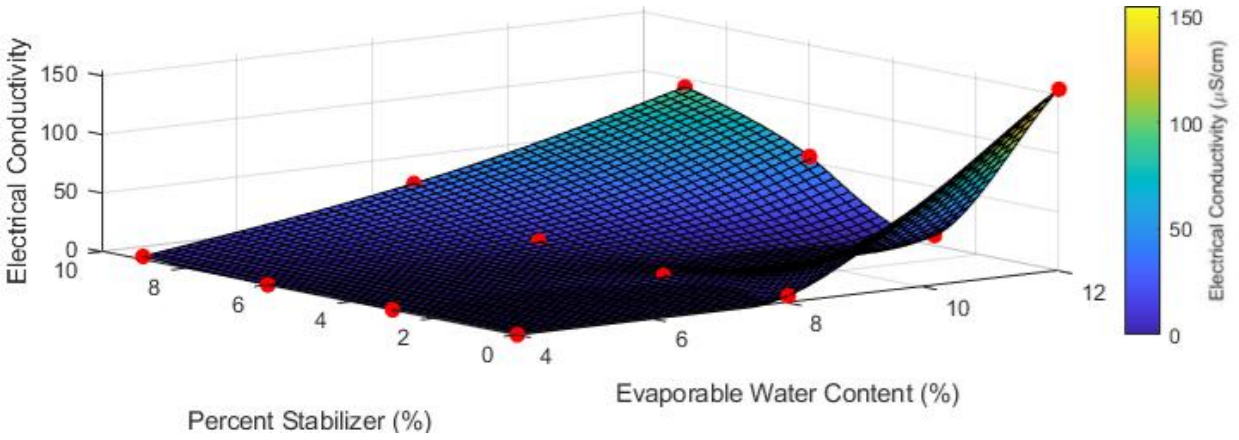

Figure 48. Graph. 3D contour plot surface for day 1 electrical conductivity.

Five FDR samples were molded at the construction design mix of 6 percent cement content with 10 percent moisture content for the UCS test. The samples were crushed in 7 days, with the average UCS value being 324 psi. According to GDOT, a minimum UCS of 450 psi is expected for laboratory samples, and, therefore, the average UCS did not meet the standard. Figure 49 displays the UCS results.

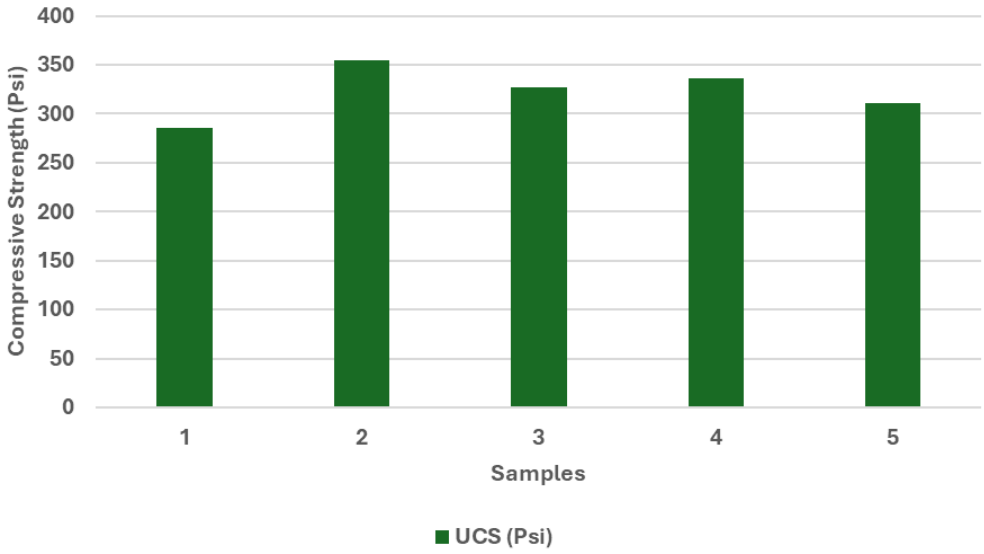

Figure 49. Graph. Results of UCS of 6 percent cement with 10 percent moisture.

In the field, the stabilized road base was scanned for 4 days, starting from the day of stabilization. The GPR dielectric constant results are shown in figure 50. They indicate a progressive decline along the stabilized pavement section. Day 1 dielectric constant was highest with values peaking above 20, suggesting high initial moisture content, surface water, and ongoing hydration of the cementitious matrix. As curing progressed to day 4, the dielectric constant decreased consistently, with values stabilizing between 9 and 13, indicating moisture reduction and increased cement hydration.

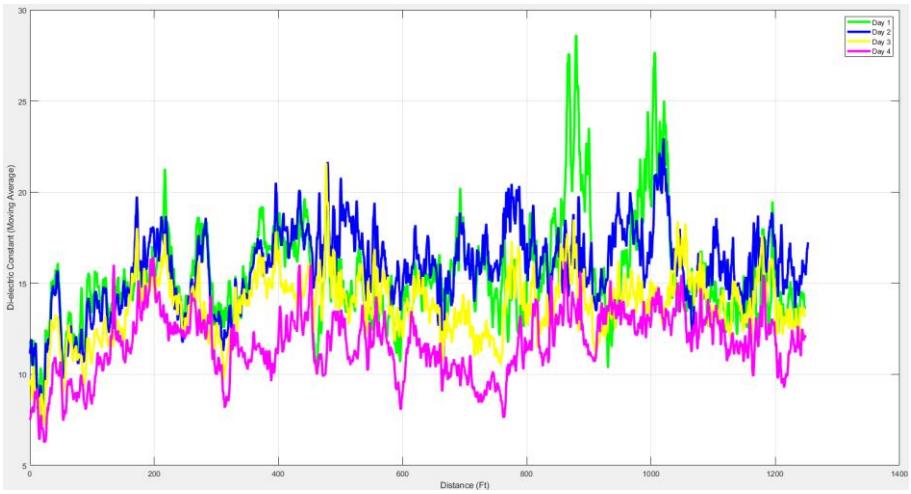

Figure 50. Graph. GPR dielectric constant results for Log House Road.

The percometer field results also confirmed that dielectric constant values were highest on day 1, reflecting high moisture content and early hydration in the FDR-stabilized base. The values declined steadily by day 3, indicating moisture loss and matrix formation. The results are shown in figure 51. Electrical conductivity showed a moderate result on day 1; spiked locally on day 2, due to the addition of moisture; and dropped sharply by day 3, suggesting ion immobilization as hydration progressed. The results are shown in figure 52.

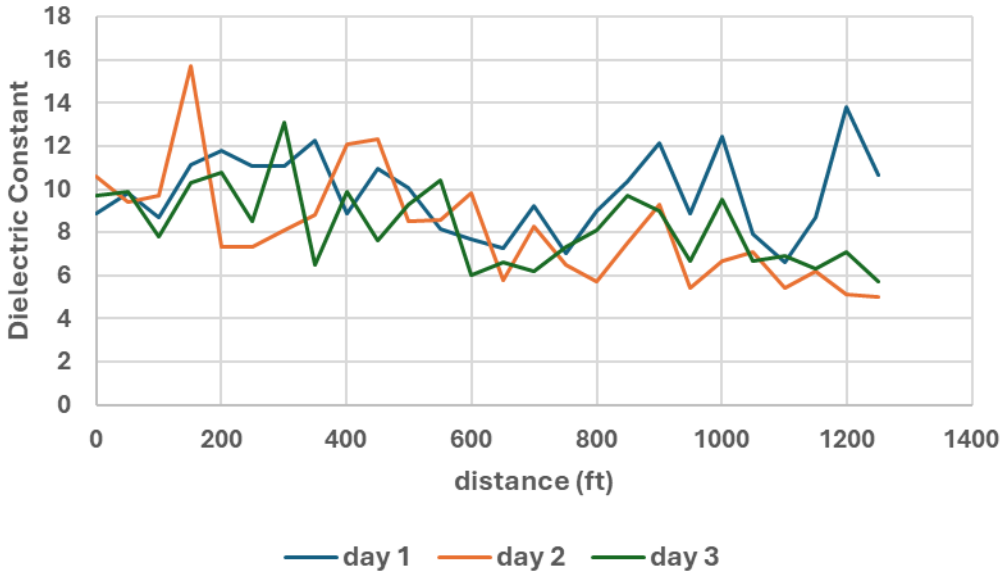

Figure 51. Graph. Field percometer results of dielectric constants for Log House Road.

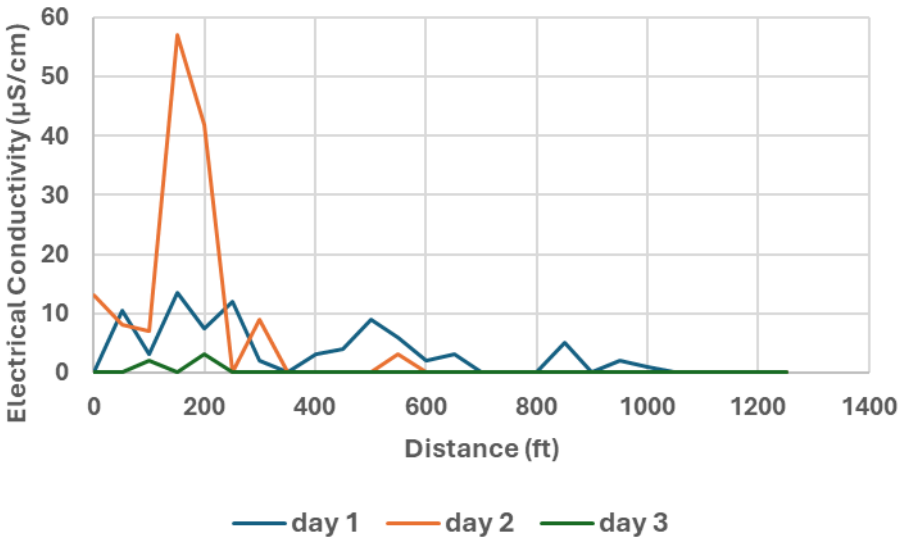

Figure 52. Graph. Field percometer results of electrical conductivity for Log House Road.

Estimated Cement Content

Figure 53 presents the results of the estimated cement content for the GPR-scanned alignment. Most of the section displayed relatively consistent cement content, ranging between 5 and 6 percent, which was within the construction design mix of 6 percent. However, several sharp dips

in cement content were observed across the profile, indicating zones of inadequate mixing or inconsistent cement application, which can compromise strength development and long-term durability.

The fluctuations also highlight possible construction quality control issues. Results for the remaining sites can be found in the appendix.

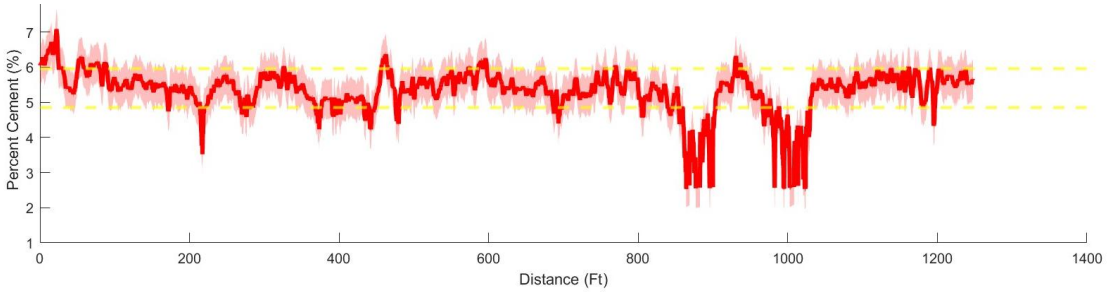

Figure 53. Graph. Results of the estimated cement content for Log House Road.

Layer Thickness

The GPR-derived layer thickness shows that the reclaimed base layer generally maintains consistency near the 10-inch design depth, with most of the profile ranging between 8 and 11 inches (see figure 54), and it is also captured in the GPR radargram scan (see figure 55). Field core samples were also taken after construction, confirming the depth ranging from 7 to 10 inches (see figure 56).

Field investigations at the remaining FDR sites were conducted using the same methodology, and the results for each site are presented in the appendix.

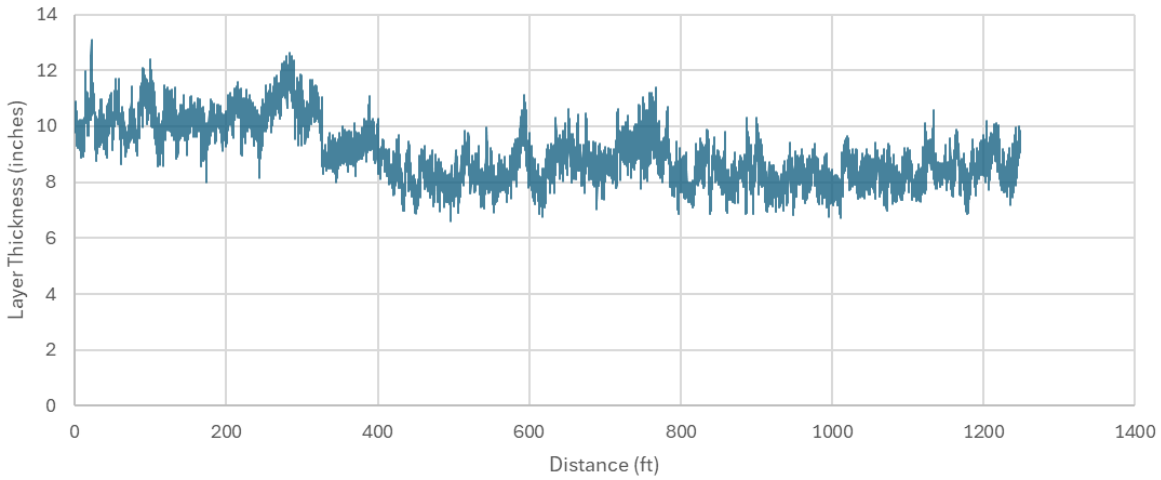

Figure 54. Graph. Layer thickness from GPR.

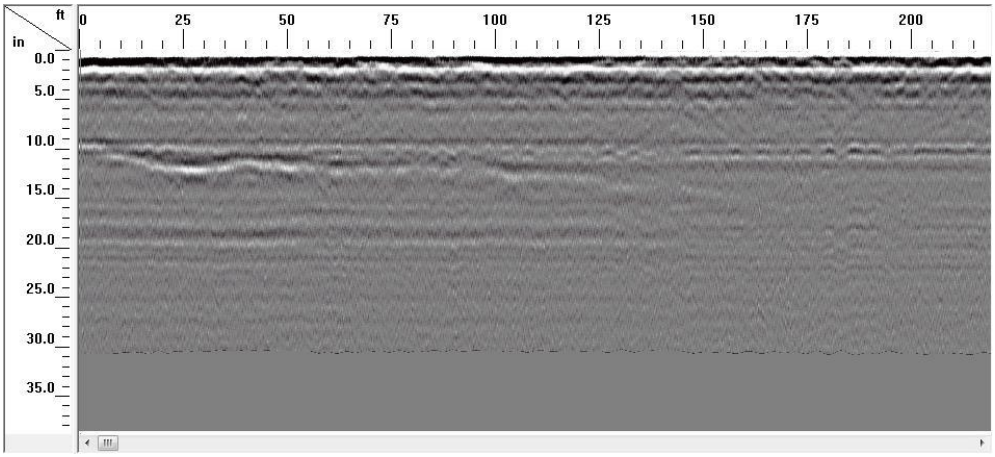

Figure 55. Image. GPR radargram scan.

Figure 56. Photos. Field core samples confirming the as-built layer thickness.

CHAPTER 7. CONSTRUCTION PROCESS AND CHALLENGES

CONSTRUCTION PROCESS

Construction with Soil-Cement

Soil from a borrow pit is tested daily to ensure the soil is within the mix design requirements. The soil is then excavated using a loader and then deposited into the hopper, where the soil is steadily dispensed onto the conveyor belt. As the soil travels through the conveyor belt, it is weighed, and the cement silo then dispenses the correct amount of cement relative to the weight of soil on the conveyor belt. Figure 57 shows a soil-cement plant.

Figure 57. Photo. Soil-cement plant.

The soil and cement are dispensed into the auger container, where mixing with the appropriate amount of water is used to achieve the mix design requirement. The soil-cement is then dispensed from the auger into the dump truck, which then takes the soil-cement to the construction site.

Construction Sequence for Full-depth Reclamation with Portland Cement

The construction of an FDR with cement-stabilized base follows a systematic sequence of operations designed to ensure uniformity, strength, and long-term durability of the treated layer. Each step plays a critical role in transforming the existing distressed pavement into a high-performance stabilized foundation that meets modern pavement design and performance standards.

The first step is milling the existing asphalt layer (see figure 58). About 2 to 3 inches of the asphalt layer is milled off, depending on the design.

Figure 58. Photo. Milling the asphaltic layer.

The process continues with cement application, where cement is uniformly distributed across the prepared roadway using a calibrated spreader truck (see figure 59). This step is critical for cement content accuracy and uniform treatment. Inconsistent application can lead to localized zones of weakness or over-stabilization, which may compromise the overall performance of the base layer.

Figure 59. Photo. Application of cement with spreader truck.

Following cement placement, pulverization and blending are performed using a rotary reclaimer (see figure 60). This self-propelled machine mills the existing pavement and underlying base materials typically to a depth of 6–16 inches and thoroughly mixes them with the applied cement. The goal is to achieve a homogeneous blend of reclaimed asphalt pavement (RAP), granular base, and cement. Uniform blending ensures consistent strength gain across the section and avoids weak interfaces between layers.

Next, the compaction phase is initiated using vibratory steel drum and pneumatic rollers. Compaction must be completed within a limited working time, often referred to as the working window, before the cement begins to set. Target densities are typically specified as a percentage of the maximum dry density (usually 95–98 percent of the modified Proctor density), and achieving uniform compaction is essential for the load-bearing performance and long-term durability of the FDR layer.

Figure 60. Photos. Reclaimer machine mixing cement with FDR base.

CHALLENGES OF FULL-DEPTH RECLAMATION CONSTRUCTION

A recurring technical issue during construction is when the reclaimer blades do not thoroughly mix the cement within the existing revolution per minute. Instead, the dry cement is pushed forward, leading to segregation (i.e., areas of excessive or insufficient cement), which can adversely affect the pavement strength and uniformity. Some of the causes include:

- *Tool geometry and condition*: Worn-out rotor and incorrect tool angles reduce penetration and shear, and thereby particles are lifted and rolled instead of being cut and mixed. This incorrect cutting depth or overlapping between adjacent passes leaves out unmixed soil. (Wirtgen 2012, Caterpillar 2010).
- *Operational parameters*: Excess forward speed during the mixing phase limits residence time and turbulence in the mixing chamber. A single pass at high speed commonly leaves a visible cement streak, especially at higher application rates.
- *Material state (moisture/gradation)*: If the layer is below optimum moisture content, particles are dusty and cohesionless. Cement has little adhesion and is easily skated forward

by the drum. Highly gap-graded or very coarse material also reduces mixing efficiency unless additional passes are made.

The consequences of these issues are uneven cement distribution, producing localized UCS and stiffness variability, which elevates the shrinkage risk. These non-uniformities appear in the estimated dielectric constant and attenuation as spatial variations, due to the GPR measuring reflection amplitudes.

CHAPTER 8. CONCLUSIONS AND RECOMMENDATIONS

CONCLUSIONS

The rate of dielectric constant decrease was determined to be a function of the cement content, water content, rate of cement hydration, and evaporation. An increase in cement content led to more free water available in the mixture being converted to chemically bound water through the cement hydration process. Consequently, more cement in the mixes led to a significant faster decrease in the dielectric constant after fabrication. The effects of an increase in water content were not strongly proportional to the decrease in dielectric constant; rather, it determined the starting dielectric constant and the likely minimum value to which the mixture will decrease to.

Field testing showed that the change in dielectric constant with time can be identified with GPR surveys conducted on the same path for multiple days after construction. This decrease was primarily controlled by the cement hydration process and the evaporation from the surface. The field results also show that the cement detection model was best suited for the first day after construction. This was due to the soil-cement/FDR being fresh and exhibiting the same dielectric constant trends as the laboratory-fabricated samples. Although it is challenging to directly correlate dielectric constant with cement content in a laboratory environment due to multiple influencing factors, the agency does not rely on dielectric constant alone to assess cement content in the field. Instead, a multivariate cement detection model was developed using two response surfaces: one relating water content, cement content, and dielectric constant, and another relating water content, cement content, and electrical conductivity. By jointly interpreting dielectric constant and electrical conductivity measured from GPR, the model accounts for the combined effects of moisture and material composition, allowing the cement content to be inferred rather than directly

measured. This approach reduces ambiguity associated with individual electromagnetic parameters and provides a defensible basis for estimating cement content from field measurements.

RECOMMENDATIONS

Based on the findings of GDOT Research Project 23-21 and the GPR-based nondestructive assessment methodology developed for evaluating cement content and stabilized layer thickness at FDR and soil-cement field sites, the following recommendations are proposed:

1. Expanded Field Implementation
    a. Apply the GPR-based methodology at multiple sites with varying soil-cement mix designs and FDR depths to validate its effectiveness in detecting cement content and stabilized layer thickness variations.
    b. Include both GDOT-standard and county-administered projects to assess quality variability, QA practices, and compliance with specifications.
2. Large Sample Testing and Verification
    a. Fabricate large-scale samples suitable for scanning with an air-coupled GPR antenna.
    b. Compare GPR readings with percometer measurements to better estimate field conditions and validate the accuracy and reliability of the cement detection model.
3. Core-based Cement Content Verification
    a. Determine cement content from hardened soil-cement cores using ASTM D806 (ASTM 2019) to validate the GPR-based model and potentially reduce the need for core testing in future applications.

b. The scope of this project did not have the means in using ASTM D806 to determine the cement content from hardened soil-cement cores. Therefore, to further strengthen the reliability and applicability of the findings from this study, continuing research is required to systematically validate the correlation between field-based nondestructive evaluation techniques and standardized laboratory test methods, including ASTM D806.

4. Field Nondestructive and Semi-Destructive Testing
    a. Conduct light weight deflectometer (LWD) and dynamic cone penetrometer (DCP) testing at selected locations following GPR surveys.
    b. Perform UCS, California bearing ratio (CBR), and resilient modulus tests alongside electrical property measurements to validate strength and stiffness predictions based on cement content and hydration rate models.
5. Application to Non-Fresh Samples
    a. Extend dielectric and electrical conductivity testing to non-fresh soil-cement samples (already in place or several weeks post-construction) to broaden the applicability of the model for post-construction QA.
6. FDR Project Monitoring
    a. Apply the developed detection methodology to FDR projects to monitor in-place cement content and stabilized layer thickness.
    b. Use data on cement distribution, layer thickness, and construction variability to establish performance-based QA specifications and inform GDOT acceptance procedures and contractor QC processes.

7. Quality Variability Management

    a. In county-administered projects, where compliance with GDOT specifications may be inconsistent, enforce robust QA/QC procedures, including uniform cement mixing, stabilized layer thickness control, and monitoring of coarse/fine aggregate fractions.
    b. Use these strengthened controls to reduce the risk of subgrade inadequacy, premature pavement distress, and failure and thereby extend pavement service life.

APPENDIX

BRIGHTON AND SAGAMORE LANE FDR SITE

The laboratory results for the dielectric constants for all mixes showed a clear and physically consistent evolution. The dielectric constant values were highest on day 1 and decreased monotonically through day 8 as free water was consumed by hydration and as specimen densified and dried. At early age, moisture content dominated the dielectric constant within each cement group, with the 12 percent water content mix exhibiting the highest dielectric constant and the 4 percent water content mixes being much lower. The day 1 result of the 3D contour plot is shown in figure 61.

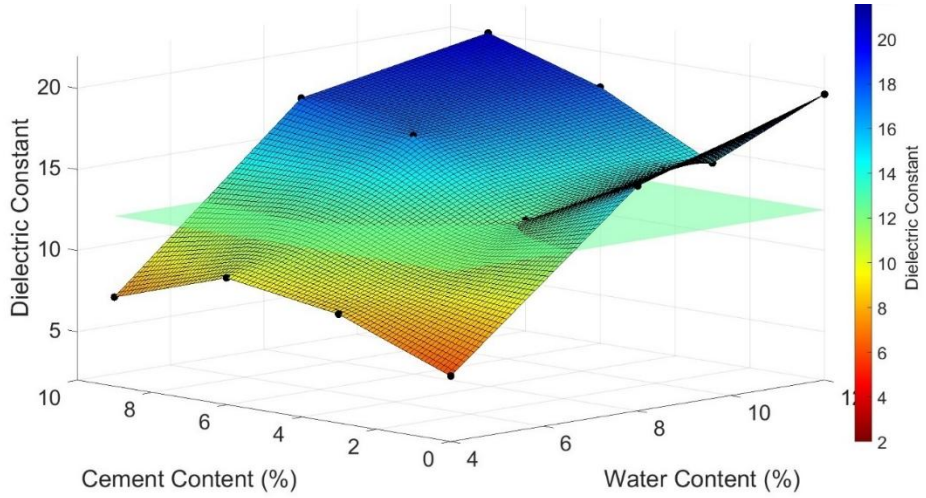

Figure 61. Graph. 3D contour plot surface for the dielectric constant for day 1 for Brighton and Sagamore Lane.

The electrical conductivity results also corroborated this interpretation, with very high electrical conductivity on day 1 for wet/high cement mixes and later collapsed to zero by days 3–5, signaling ion immobilization and pore refinement. The day 1 result is shown in figure 62.

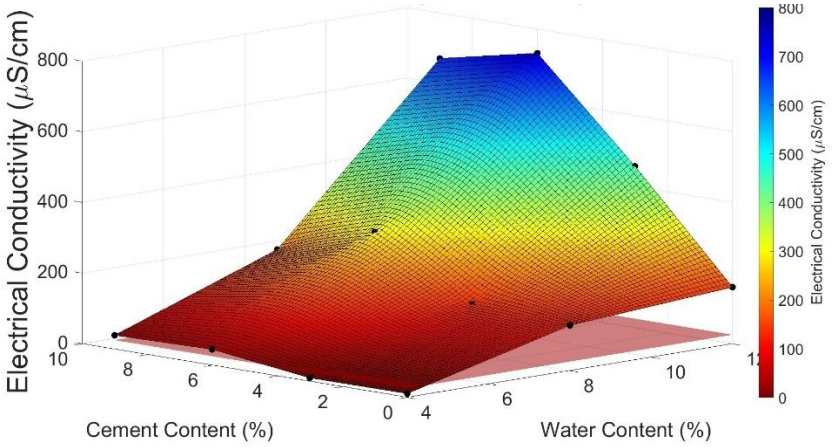

Figure 62. Graph. 3D contour plot surface for electrical conductivity for day 1 for Brighton and Sagamore Lane.

The results of the GPR dielectric constant profile showed a clear decrease and stabilization from day 1 to day 2, with values generally dropping from 9 to 16 on day 1 to between 8 and 12 on day 2 (see figure 63). This behavior is consistent with early hydration. The free water and mobile ions present immediately after mixing increased the dielectric constant on day 1, and by day 2, consumption of free water occurred, reducing the dielectric constant.

Spatial patterns of higher dielectric constant and lower dielectric constant persist across the days, indicating construction variability (i.e., moisture conditioning or mixing efficiency).

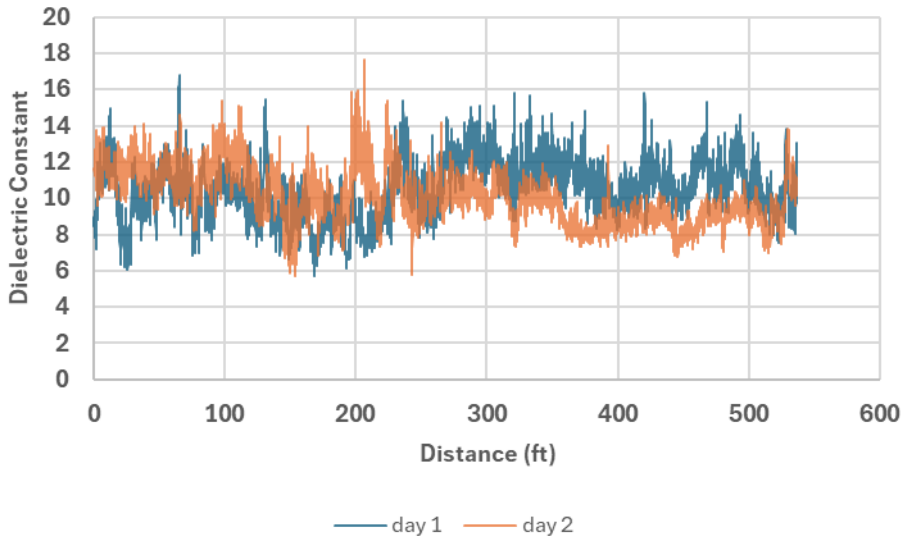

Figure 63. Graph. GPR dielectric constant results for Brighton and Sagamore Lane.

Percometer spot tests along the stabilized road showed the early age EM evolution as high dielectric constant on day 1, reflecting free water and mobile ions in the pore fluid, and dropped uniformly by days 2 and 3 as hydration binds water into C-S-H/AFT and moisture gradients diminish (see figure 64). Figure 65 denotes electrical conductivity exhibited sharp, localized spikes on day 1 followed by a rapid collapse toward zero by day 3, indicating ion immobilization and pore refinement.

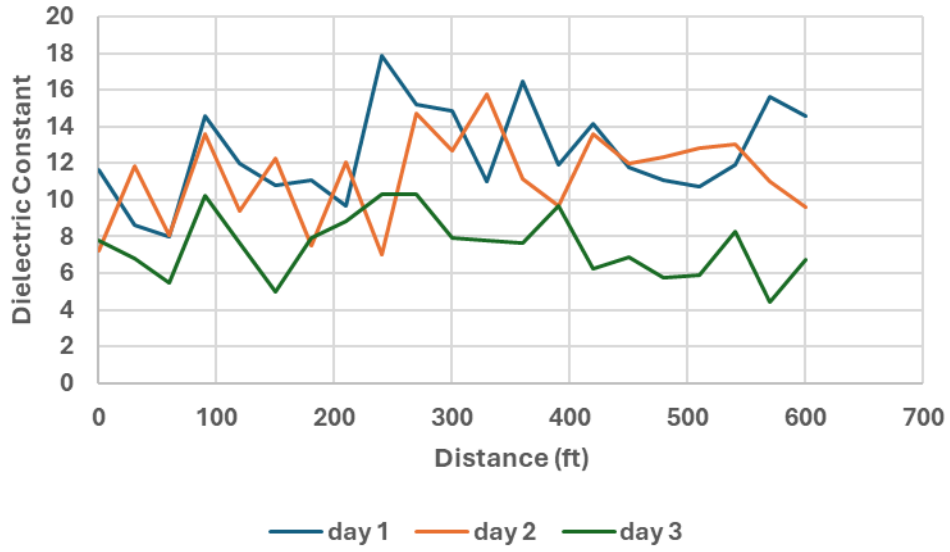

Figure 64. Graph. Field percometer results for the dielectric constant for Brighton and Sagamore Lane.

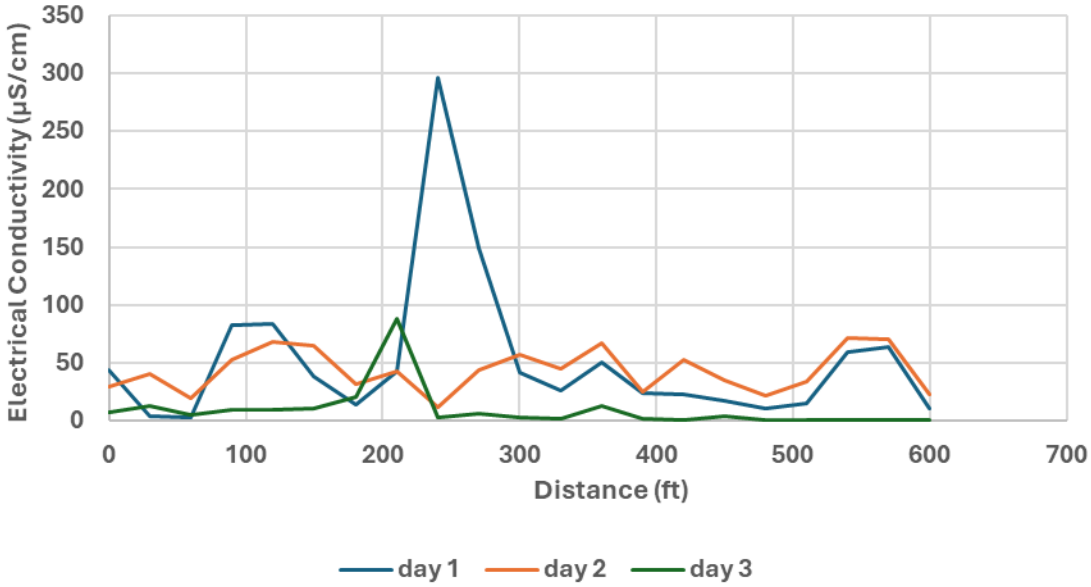

Figure 65. Graph. Field percometer results for electrical conductivity for Brighton and Sagamore Lane.

The estimated cement content results demonstrate considerable spatial variability along the scanned alignment (see figure 66). Although the design mix target was set at 5.5 percent cement content, the results revealed the majority of the section fluctuates between 6 and 6.8 percent, with

frequent peaks reaching up to 9 percent in certain areas. This suggests potential over-application of cement in some zones, likely resulting from inconsistent spreader calibration or variability in reclaimer performance.

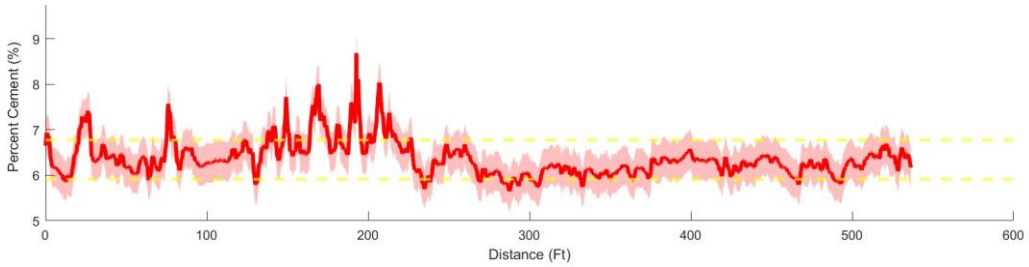

Figure 66. Graph. Results of the estimated cement content for Brighton and Sagamore Lane.

Layer Thickness

The GPR-derived layer thickness results indicate a uniform FDR base with most of the profile maintaining values close to the 10-inch design thickness. The thickness values fluctuate narrowly between approximately 8 and 11 inches, showing good control of the reclaimer depth (see figure 67).

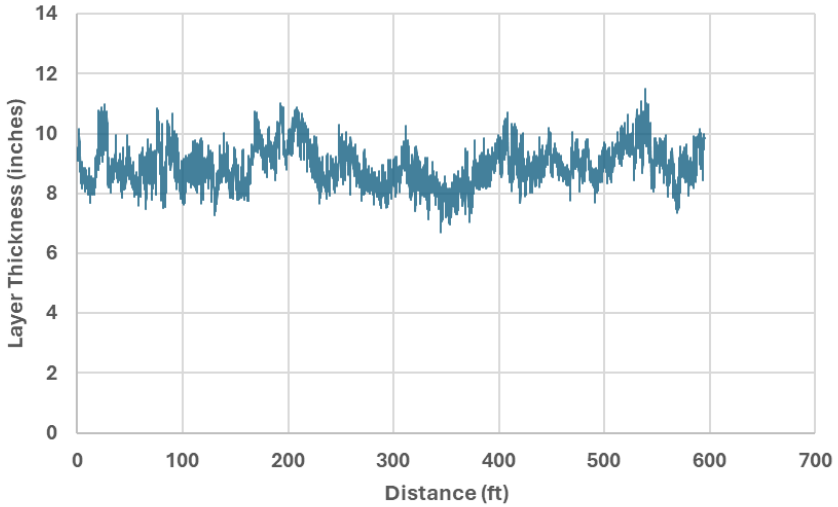

Figure 67. Graph. Layer thickness from GPR.

OLD COVINGTON ROAD FDR SITE

The 3D contour surface plot of the laboratory dielectric constant for day 1 is shown in figure 68, and that of electrical conductivity for day 1 is shown in figure 69. The dielectric constant surface showed a gradual increase, with rising water content across all cement levels, highlighting the dominant influence of moisture on permittivity. Lower cement contents paired with higher moisture contents yielded the highest dielectric constant due to the presence of unbound water and early-stage ionic mobility.

The electrical conductivity surface exhibited a sharp peak around 6 percent cement and 12 percent moisture content, indicating intense ionic activity during early hydration. As cement content increased beyond this range, conductivity dropped sharply.

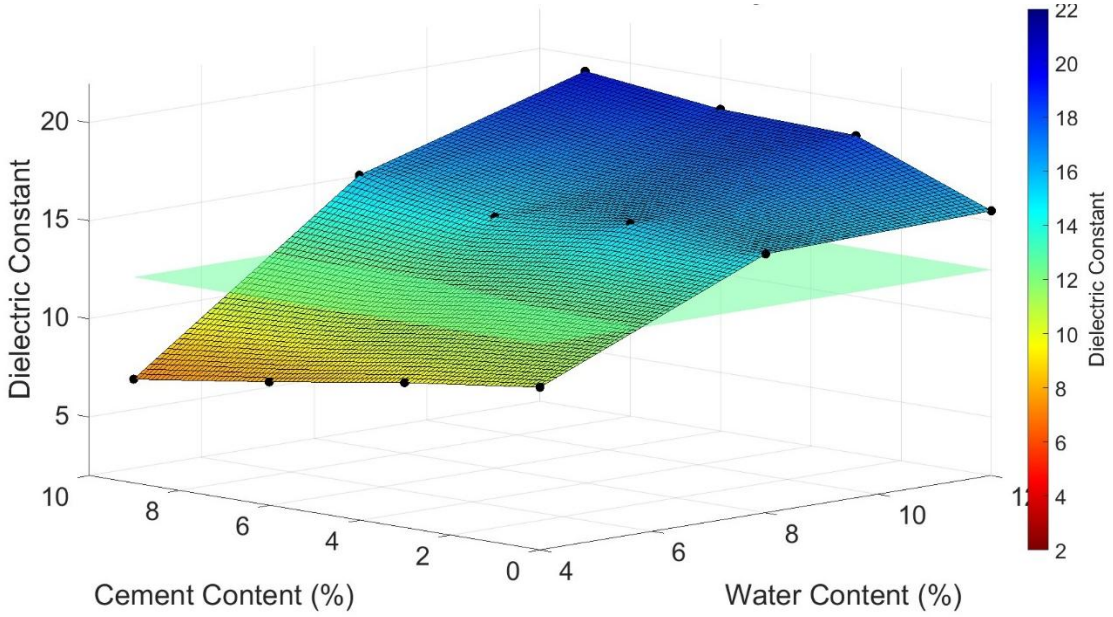

Figure 68. Graph. 3D dielectric constant contour surface for day 1 for Old Covington Road.

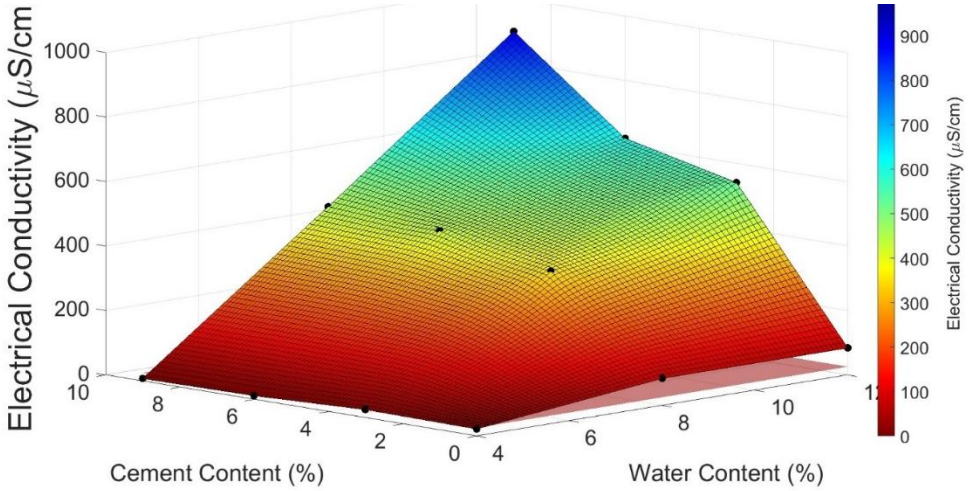

Figure 69. Graph. 3D electrical conductivity contour surface for day 1 for Old Covington Road.

The GPR dielectric constant results for days 1 and 2 exhibit a clear temporal decline, consistent with expected cement hydration behavior in the early curing stages of the stabilized base. On day 1, dielectric constant values were generally higher and more variable, with several spikes indicating elevated moisture content and high ionic mobility from unbound water and early hydration products. By day 2, dielectric values were more stabilized and reduced, suggestive of progressive moisture consumption and increased bound water as cement hydration advanced. The results are shown in figure 70.

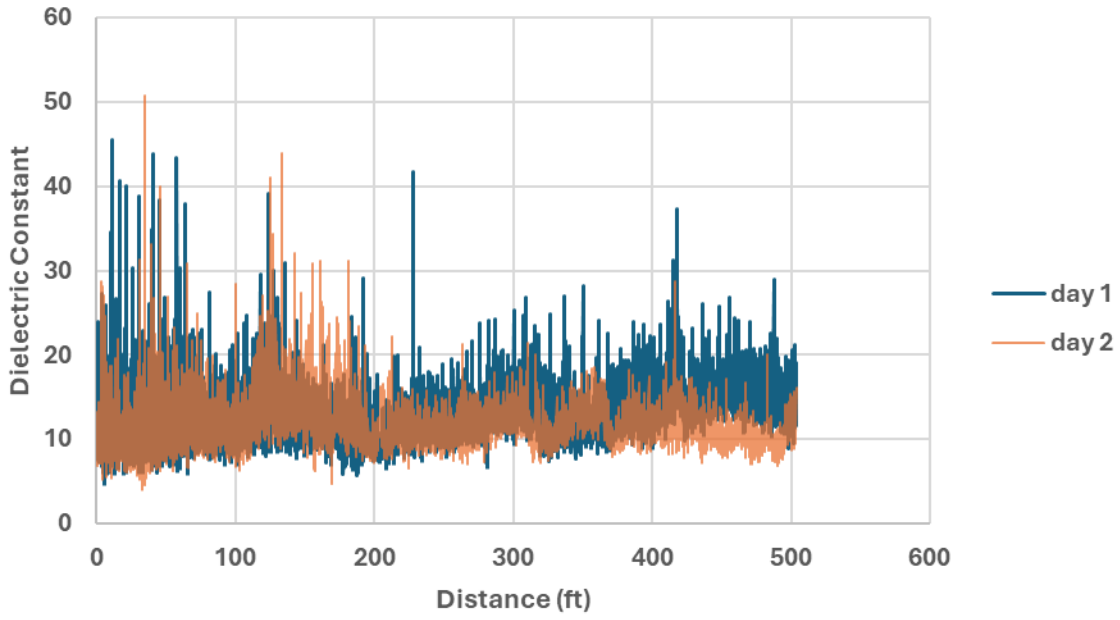

Figure 70. Graph. GPR dielectric constant result for Old Covington Road.

Based on the field percometer results for the dielectric constant (see figure 71) and electrical conductivity (see figure 72), the data reflect the early hydration behavior of the cement-stabilized base layer.

On day 1, the dielectric constant values were relatively higher at 105 and 420 ft along the scanned alignment, indicating elevated moisture content and the presence of free water. The electrical conductivity also showed significantly higher values across the alignment, peaking above 100 µS/cm, signifying high ionic concentration.

On day 2, both the dielectric constant and electrical conductivity values showed a noticeable decline at several intervals.

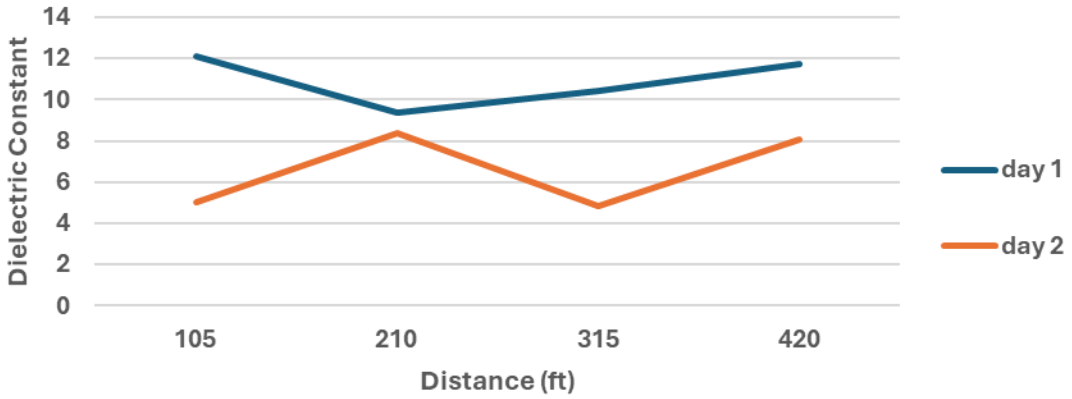

Figure 71. Graph. Field percometer results for the dielectric constant for Old Covington Road.

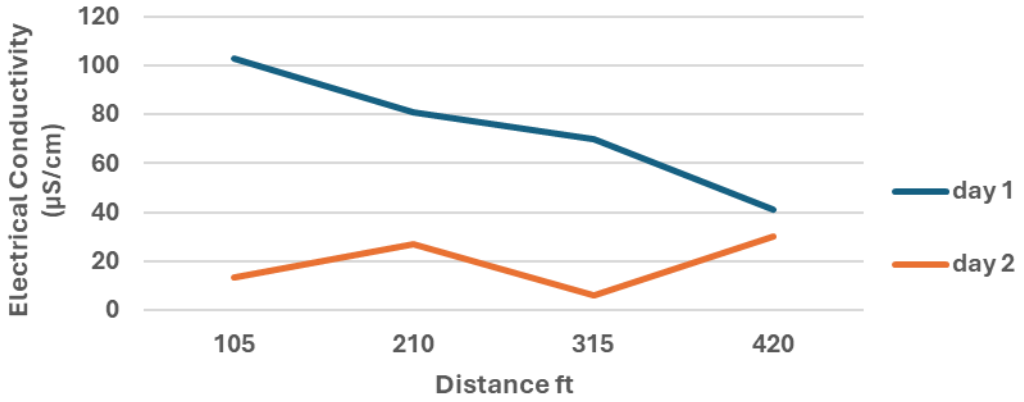

Figure 72. Graph. Field percometer results for electrical conductivity for Old Covington Road.

The results of the estimated cement content profile for Old Covington Road (see figure 73) demonstrate both spatially consistent and notable localized variability across the pavement section. The estimated cement content values oscillate around 5.2–6.5 percent, which is a bit higher than the designed mix of 5.3 percent. However, significant short-range fluctuations were evident, with sharp dips below 4 percent and spikes exceeding 7 percent in several areas. These deviations suggest zones of non-uniform mixing, possibly due to field construction factors.

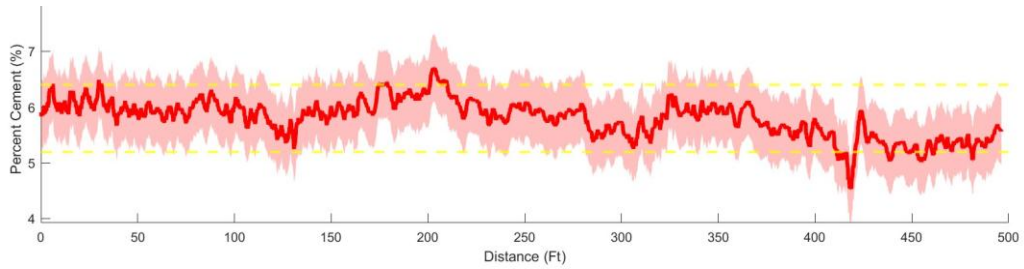

Figure 73. Graph. Results of the estimated cement content for Old Covington Road.

DANIELS BRIDGE ROAD FDR SITE

The GPR dielectric constant results (see figure 74) decreased from day 1 to day 2, reflecting typical early stage curing behavior of cement-stabilized bases. Day 1 results exhibited higher dielectric constant values, especially at localized peaks, indicating elevated moisture and free ions shortly after mixing. By day 2, the dielectric constant values dropped uniformly, suggesting moisture reduction due to hydration.

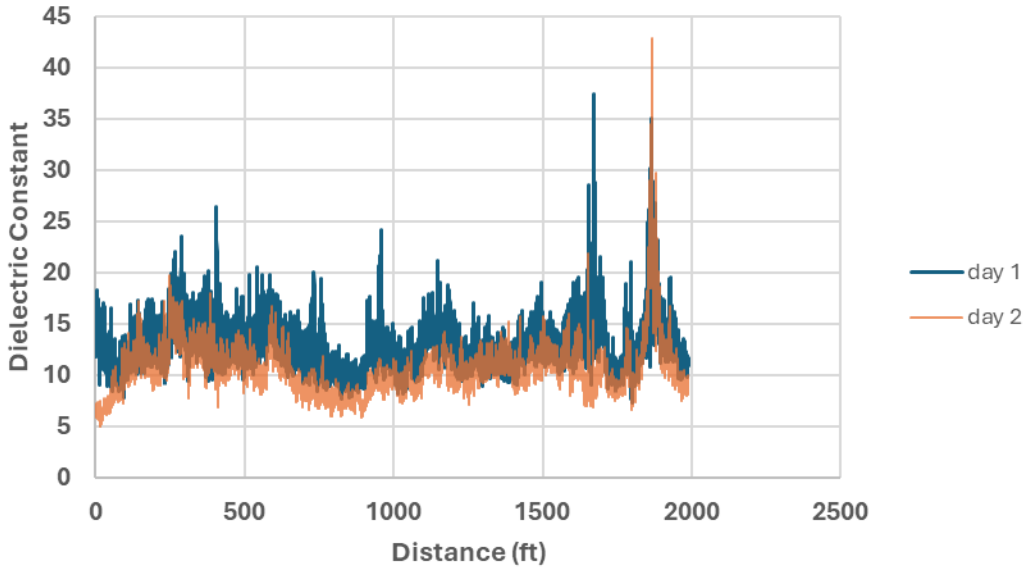

Figure 74. Graph. GPR dielectric constant result for Daniels Bridge Road.

The percometer field results for the dielectric constant and electrical conductivity are shown in figure 75 and figure 76, respectively. The dielectric constant generally declined from day 1 to day 3, indicating moisture reduction and progressive cement hydration. Day 1 values mostly ranged between 7 and 11, whereas day 2 showed greater fluctuation, including a sharp peak at around 540 ft, possibly indicating an area of excess moisture or poor blending. By day 3, dielectric constants stabilized, generally showing lower values and reduced variability.

Similarly, the electrical conductivity data showed distinct peaks on day 2, as seen around 540 ft along the scanned alignment, that reached above 30 µS/cm, suggesting localized ionic concentration, which is likely due to unreacted cement or excessive water. Day 1 and 3 values remained relatively low overall, confirming rapid ion consumption and pore refinement as hydration progresses.

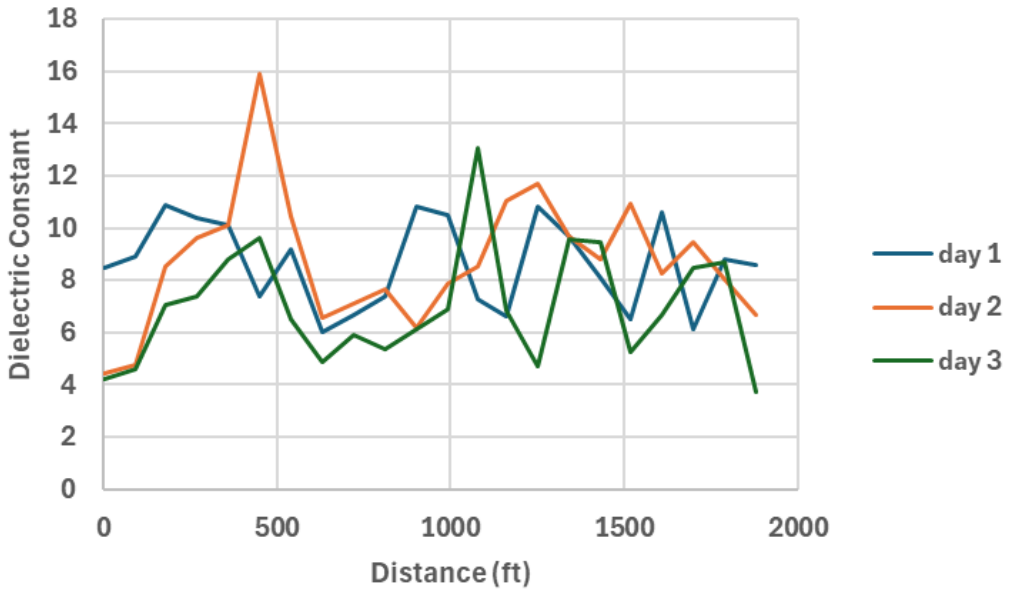

Figure 75. Graph. Field percometer results for the dielectric constant for Daniels Bridge Road.

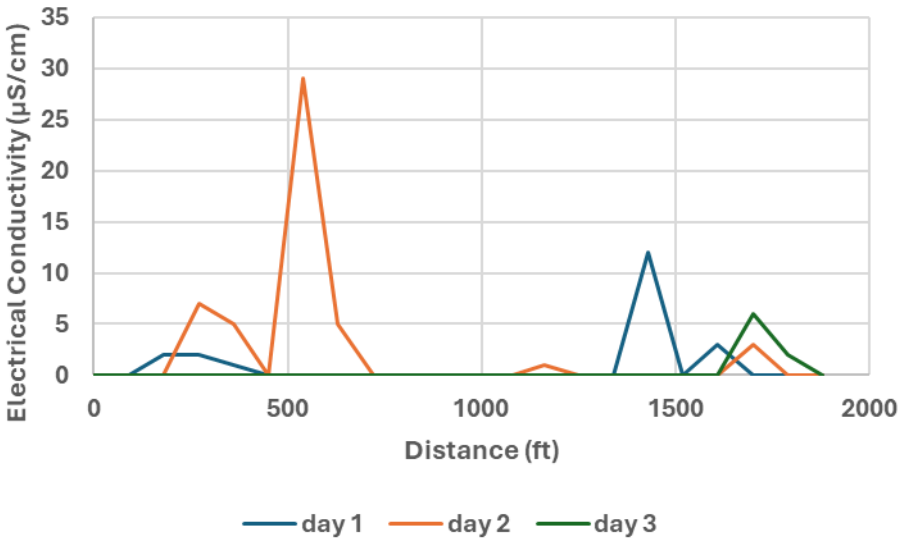

Figure 76. Graph. Field percometer results for electrical conductivity for Daniels Bridge Road.

The estimated cement content results along the Daniels Bridge Road alignment showed a consistent trend centered around 5.3–6.3 percent, slightly above the 4.8 percent design target. This suggests overall sufficient cement content for structural performance, but the presence of frequent short dips below 4 percent and occasional spikes above 7 percent indicates localized variability. These deviations may result from construction factors such as spreader inconsistencies and mixing inefficiencies. The results are shown in figure 77.

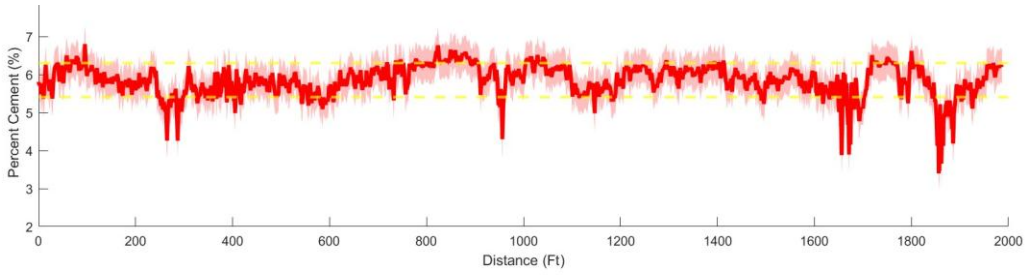

Figure 77. Graph. Results of the estimated cement content for Daniels Bridge Road.

ATLANTA MOTOR SPEEDWAY FDR SITE

The 3D contour surface results for the day 1 dielectric constant and electrical conductivity are shown in figure 78 and figure 79, respectively. The results illustrate the strong interdependence between moisture and cement content in the early-stage FDR cement mix behavior. The general trend observed was a decrease in dielectric constant and electrical conductivity during the curing days. Cement content had a subtler impact on dielectric constant after mixing, suggesting that before hydration progresses, water dominates the EM response. The electrical conductivity surface exhibits a sharp peak at low cement and high moisture content, highlighting intense ionic activity due to unbound ions before cement hydration products begin to form. As cement content increased, conductivity sharply declined, reflecting early ionic immobilization through hydration. These trends confirm that on day 1, the dielectric constant is most responsive to moisture, whereas conductivity captures ionic availability and early hydration onset.

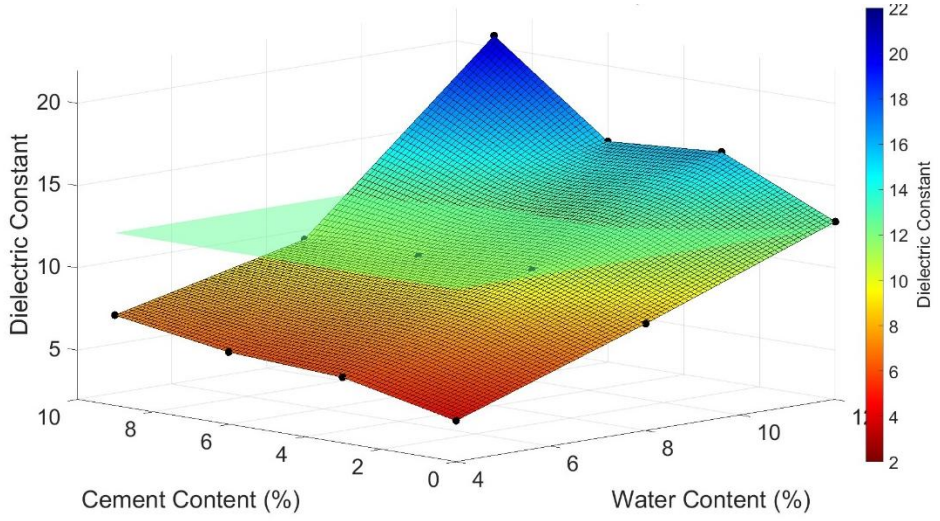

Figure 78. Graph. 3D dielectric constant contour surface for day 1 for Atlanta Motor Speedway.

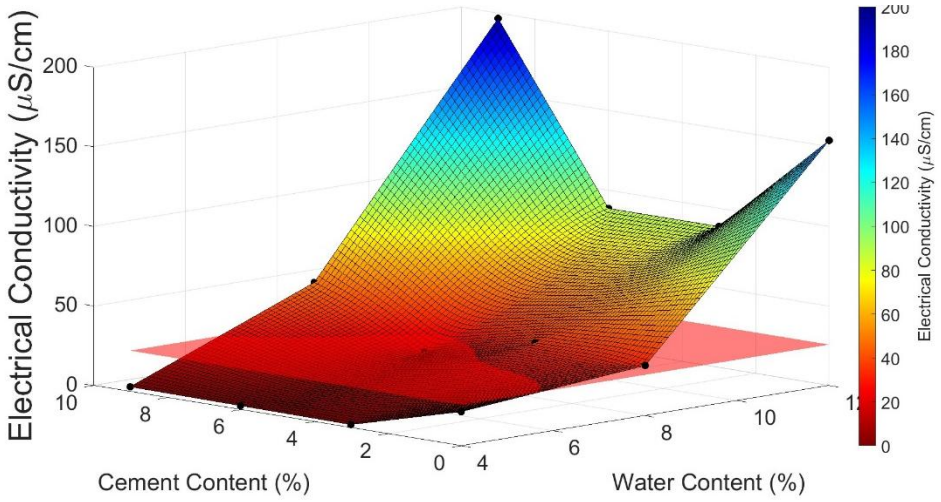

Figure 79. Graph. 3D electrical conductivity contour surface for day 1 for Atlanta Motor Speedway.

The results of the GPR dielectric constant are shown in figure 80. Day 1 results exhibit the highest and most variable dielectric constant exhibited by free moisture and mobile ions immediately after mixing. By day 2, the dielectric constant decreased overall but remained locally inconsistent, indicating ongoing hydration and a few wetter zones that have equilibrated. By day 3, it stabilized and dropped to a narrow band, reflecting moisture loss and formation of low permittivity hydration product.

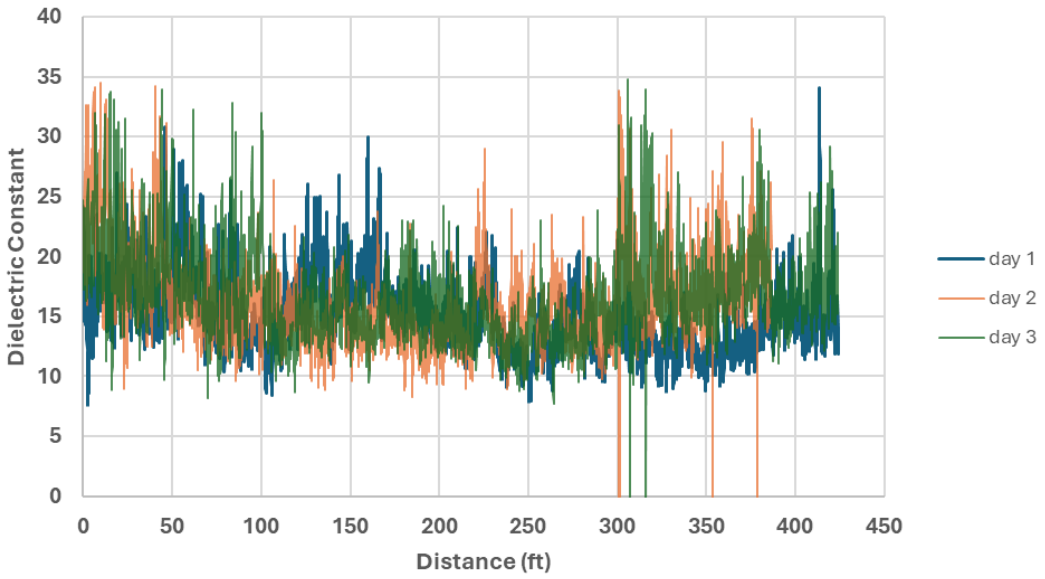

Figure 80. Graph. GPR dielectric constant result for Atlanta Motor Speedway.

The results of the estimated cement content are shown in figure 81. Across the alignment, the estimated cement content fluctuates around a trend of roughly 4–6 percent, which is within the 4 percent design mix, with short-length spikes up to 6.5 percent and occasional dips toward 3.5 percent. This pattern points to adequate average cement content application but localized variability.

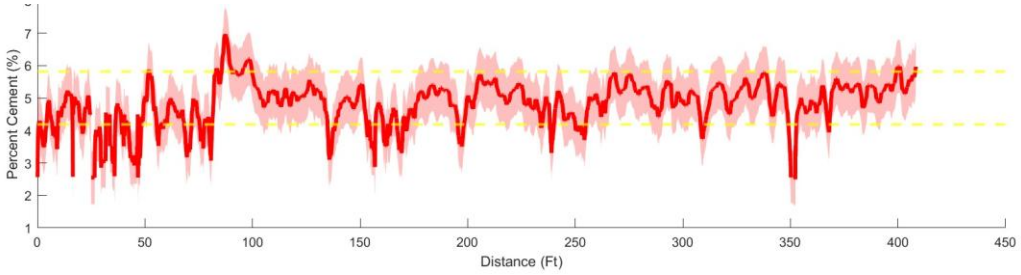

Figure 81. Graph. Results of the estimated cement content for Atlanta Motor Speedway.

REFERENCES

Al-Qadi, I. L., & Lahouar, S. (2005). Measuring layer thicknesses with GPR – Theory to practice. Construction and Building Materials, 19(10), 763–772. https://doi.org/10.1016/j.conbuildmat.2005.06.005

American Association of State Highway and Transportation Officials. (2023). AASHTO T27 - 23: Standard method of test for sieve analysis of fine and coarse aggregates. Washington, DC:

ASTM International. (2019). ASTM C136/ C136M - 19: Standard test method for sieve analysis of fine and coarse aggregates. West Conshohocken, PA: ASTM International.

ASTM International. (2019). ASTM D806 - 19: Standard test method for cement content of hardened soil - cement mixtures. West Conshohocken, PA: ASTM International.

ASTM International. (2021). ASTM D698 - 12 (2021): Standard test methods for laboratory compaction characteristics of soil using standard effort (12,400 ft-lbf/ft3 {600 KN-m/m3} (Standard Proctor). West Conshohocken, PA: ASTM International.

Barnes, C. L., Haque, R., Salah, P., & Alward, C. (2012). Control of full depth pulverized aggregate production using ground penetrating radar (Paper No. 2012 - 401). In 2012 Conference and Exhibition of the Transportation Association of Canada: Transportation Innovations and Opportunities. Ottawa, ON: Transportation Association of Canada.

Bell, F. G. (1996). Lime Stabilization of Clay minerals and Soils. Engineering Geology, 42(4), 2

Benedetto, A., & Pajewski, L. (Eds). (2015). Civil Engineering Applications of Ground Penetrating Radar. Springer.

Caterpillar Inc. (2010). RM Series reclaimer/stabilizer: Operations & maintenance manual. Peoria, IL: Caterpillar Inc.

Consoli, N. C., Foppa, D., Festugato, L., & Heineck, K. S. (2007). Key parameters for strength control of artificially cemented soils. Journal of Geotechnical and Geoenvironmental Engineering, 133(2), 197–205.

Crockford, B. D., Deng, T., Devadas, A., Gu, F., Im, S., Joshaghani, A., Wilson, B. (2021). Develop rapid quality control and assurance technologies for pavements: Phase II report (FHWA/TX-21/0-6874-R2). College Station, TX: Texas A&M Transportation Institute; Austin, Texas: Texas Department of Transportation.

Daniels, D. J. (2004). Ground penetrating radar (2nd ed.). London, UK: The Institution of Engineering and Technology.

Daniels, D. J. (2009). Chapter 4 - Antennas. In H. M. Jol (Ed.), Ground penetrating radar: Theory and applications (pp. 99 - 139). Amsterdam, The Netherlands: Elsevier.

Fedrigi, W., Nunez, W. P., & Visser, A. T. (2020). A review of full-depth reclamation of pavements with Portland cement: Brazil and abroad. Construction and Building Materials, 262, 120540 (Elsevier).

Federal Highway Administration (FHWA). (2011). TechBrief: Blended and performance cements (FHWA-HIF-11-025). Washington, DC: US. Department of Transportation, Federal Highway Administration.

Fleming, M. I. (2013). Full-depth reclamation: A roadway rehabilitation technique using green technology. Harrisburg, PA: Pennsylvania Department of Transportation.

Geophysical Survey Systems, Inc. (GSSI). (2023). Radan 7 user manual. Nashua, NH: Author.

Halsted, G. E., Adaska, W. S., & McConnell, W. T. (2008). Guide to Cement - modified soil (CMS) (EB242). Skokie, IL: Portland Cement Association.

Hartman, M., & Tazik, M. (2016). Full-depth reclamation (FDR) for suburban/urban and local roads application. (MN/RC 2016-25). St. Paul, MN: Minnesota Department of Transportation.

Hartman, A. (2016). Performance of cement stabilized layers for pavement rehabilitation. (Report 0-6740-1) College Station, TX: Texas A&M Transportation Institute.

Hausmann, M. R. (1990). Engineering principles of ground modification. New York, NY: McGraw-Hill.

Huisman, J. A., Hubbard, S. S., Redman, J.D., & Annam, A. P. (2003). Measuring soil water content with ground penetrating radar: A review. Vadose Zone Journal, 2(4), 476-491.

Humboldt Manufacturing Company. (2017). H-4112 Percometer manual. Elgin, IL: Humboldt Mfg. Co.

Kargas, G., Popescou, P., Kaliontzis, N., Marougas, D., & Kerkides, P. (2017). Estimation of the electrical conductivity of saturated paste extract using a dielectric sensor. Journal of Irrigation and Drainage Engineering, 143(5), 04016086

Kaya, A., & Fang, H. Y. (1997). Identification of contaminated soils by dielectric constant and electrical conductivity. Journal of Environmental Engineering, 169–177.

Kim, S., Kang, J., Lee, S. H., & Ahn, Y. H. (2016). Effect of chlorides on conductivity and dielectric constant of hardened cement mortar: NDT for durability evaluation. Advances in Materials Science and Engineering, 2016, 6018476.

Kwon, J., Seo, Y., Kaplan, A., & Yang, J. (2020). Full-depth pavement reclamation: Performance assessment and recommendations for best performance. Atlanta, GA: Georgia Department of Transportation.

Leng, Z., & Al-Qadi, I.L. (2014). An innovative method for measuring pavement dielectric constant using the extended CMP method with two air - coupled GPR systems. NDT & E International, 66, 90 - 98.

Little, D. N. (1995). Handbook for stabilization of pavement subgrades and base courses with lime. Arlington, VA: National Lime Association.

Loulizi, A., Al-Qadi, I. L., Lahouar, S. (2003). Optimization of ground-penetrating radar data to predict layer thicknesses in flexible pavements. Journal of Transportation Engineering, 93–99.

Luhr, D. R., Adaska, W. S., & Gress, D. L. (2005). Guide to full-depth reclamation (FDR) with cement.(EB234) Skokie, IL: Portland Cement Association.

Mitchell, J. K., & Soga, K. (2005). Fundamentals of soil behavior (3rd ed.). Hoboken, NJ: Wiley.

Portland Cement Association (PCA). (2020). Guide to Cement - stabilized subgrade soils (SR1007P). Skokie, IL: Athor.

Pokkuluri, K. (1998). Effect of admixtures, chlorides, and moisture on dielectric properties of Portland cement concrete in low microwave frequency range (Master's thesis). Virginia Polytechnic Institute and State University, Blacksburg, VA.

Redman, J. D., Davis, J.L., Galagedara, L. W., & Parkin, G. W. (2002). Field studies of GPR air launched surface reflectivity measurements of soil water content. In Proceedings of SPIE: Ninth International Conference on Ground Penetrating Radar (Vol. 4758, pp. 156 - 161). Bellingham, WA: SPIE. https://doi.org/10.1117/12.462256

Reeder, G. D., Harrington, D., Ayers, M. E., Adaska, W. S. (2017). Guide to full depth reclamation (FDR) with cement (SR1006P; reprinted 2019). Ames, IA: National Concrete Pavement Technology Center, Iowa State University; Skokie, IL: Portland Cement Association.

Saha, S. (2019). Characterization of unbound and stabilized materials and improved consideration of their effects on pavement performance (Doctoral dissertation). Texas A&M University.

Sherwood, P. (1993). Soil stabilization with cement and lime: State of the art review (TRL Report 332). Crowthorne, UK: Transport Research Laboratory.

Tosti, F., & Slob, E. C. (2015). Determination by using GPR of the volumnetric water content in structures, foundations and soil. In A. Benedetto & L. Pajewski (Eds.), Civil engineering applications of ground penetrating radae (pp. 163-194). Charm, Switzerland: Springer.

Wirtgen. (2012). Cold recycling and soil stabilization: Technology & application. (Cold Recycling Manual/ WR series). Windhagen, Germany: Wirtgen Group.